Available online at www.CivileJournal.org

Civil Engineering Journal

(E-ISSN: 2476-3055; ISSN: 2676-6957)

Vol. 9, No. 02, February, 2023

Shear Strength of Reinforced Concrete Squat Walls

Ahmed Faleh Al-Bayati [1*]

[1] Assistant professor, Department of Civil Engineering, Al-Nahrain University, P.O. Box:64040, Jadriah, Baghdad, Iraq.

Received 09 November 2022; Revised 28 December 2022; Accepted 17 January 2023; Published 01 February 2023

Abstract

Squat shear walls are widely used in various structures to resist earthquake loads. However, the relevant design expressions found in building codes and literature do not incorporate the influence of all crucial parameters and provide inconsistent peak shear strength estimations. This study adopts the artificial neural network (ANN) to predict the peak shear strength of squat walls using an extensive database that includes the results of 487 walls with wide-ranging test parameters. The ANN models consider the effect of concrete strength, the wall aspect ratio, vertical and horizontal reinforcements, vertical reinforcement of boundary elements, and axial load ratio. These accurately predicted the available test results. They implemented it to carry out parametric and sensitivity analysis to investigate the effect of the main parameters on the peak strength and to give information about the factors that contribute most to the shear response. In addition, a softened strut and tie method is proposed, considering the variables that substantially influence the shear strength. A nonlinear regression analysis is employed to determine the coefficients of the proposed model using the available database. The performance of the proposed model is measured using the existing models, which results in the best favorable agreement with the test results.

Keywords: Reinforced Concrete; Squat Walls; Seismic Design; Artificial Neural Network; Strut and Tie Method.

1. Introduction

Reinforced concrete (RC) structural walls find wide application in various buildings to enhance their seismic capacity by increasing lateral stiffness and minimizing lateral deformations. The slender RC walls develop their flexural strength to maintain the life-safety of a structure and reduce the damages when subjected to severe earthquakes [1], and the proper design and detailing demand ductile behavior and avoid brittle shear failure under seismic loads [2]. But this is not the case for short walls (squat walls) having an aspect ratio equal to or less than 2, as the behavior is controlled by shear deformations [3]. Squat walls are utilized in nuclear facilities, low-rise buildings, podiums of high-rise buildings, and bridges as principal structural members for lateral load resistance owing to their high stiffness and capability to limit lateral deformations [4]. Since the strength of squat walls is determined by shear instead of flexural, an appropriate estimation of the peak shear strength is crucial in designing such walls to guarantee ductile performance and avoid undesirable shear failure under earthquakes [5].

The behavior of squat walls has received considerable attention over the last few decades, and extensive experimental work has been conducted to aid in the understanding of such behavior [6–11]. They concluded that parameters such as the wall's aspect ratio, axial load, concrete strength, vertical and horizontal reinforcements, and boundary elements have a pronounced influence on peak shear strength [12, 13]. Despite the popularity of squat walls and thorough investigations, the current methods in the design codes remained unchanged for decades [14]. These methods consider different parameters, do not reflect physical behavior, and provide scattered strength predictions when estimating the test results [14]. Therefore, there is a need to develop a reliable model to predict peak shear strength.

* Corresponding author: ahmed.f.al-bayati@nahrainuniv.edu.iq

http://dx.doi.org/10.28991/CEJ-2023-09-02-03

To address the aforementioned problem, several models in various forms are developed based on various methods. For instance, Wood [15], Sanchez-Alejandre and Alcocer [16], and Gluec & Whittaker [17] suggested empirical expressions. On the contrary, Hsu & Mo [18], Massone & Melo [19], and Chandra et al. [12] developed softened truss models. Hwang & Lee [20, 21], Kassem [14], Ma et al. [22], and Chetchotisak et al. [23] presented strut and tie models. Although the accuracy of the above models is improved compared to the design codes, some still provide inconsistent strength predictions because they are derived using a limited number of experimental results. Furthermore, some of these models are devoted exclusively to rectangular walls and provide scattered estimations when applied to calculate the shear strength of flanged walls [22]. The models of Gluec & Whittaker [17], and Ma et al. [22], on the other hand, are derived solely to predict the shear strength of flanged walls.

The current progress in the machine learning field opened new perspectives to develop more reliable computer programs to predict the peak shear strength of squat walls. For example, Chen et al. [24] employed artificial neural networks (ANN) and particle swarm optimization (PSO) to develop a hybrid model for the shear strength of rectangular squat walls. Baghi et al. [25] suggested an empirical model using the PSO technique. Gondia et al. [26] and Tariq et al. [27] introduced expressions to calculate the shear strength of flanged squat walls using genetic programming (GP) and gene expression programming (GEP) techniques, respectively. While Feng et al. [28] and Parsa & Naderpour [29] developed shear strength predictive models for flanged squat walls using the *eXtreme Gradient Boosting* (XGBoost) algorithm and improved support vector regression method (SVR), respectively.

This work is a new attempt to predict the peak shear strength of rectangular and flanged squat walls. Unlike the previous studies, the current one employs a substantial database of 487 squat walls that experienced shear failure with a broad range of test variables to build ANN and the strut and tie models. Since the predicted peak strength by the ANN models is made using non-accessible matrices, they are utilized to conduct parametric and sensitivity analysis to study the influence of the geometric and mechanical variables and measure their contribution to peak shear strength for rectangular and flanged walls. The strut and tie method is applied to develop a simplified model replicating the load transfer mechanism to calculate the shear strength of rectangular and squat walls. The performance of the proposed model is gauged with those of the existing ones. Figure 1 summarizes the workflow of this research.

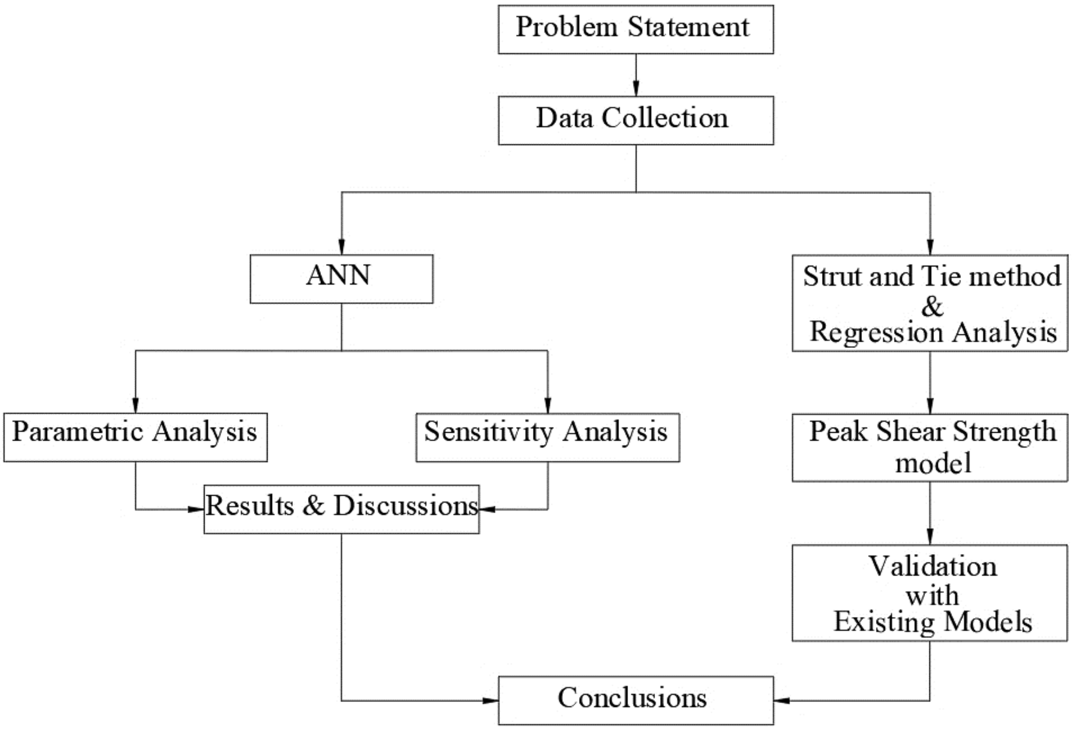

Figure 1. Research workflow

2. Squat Shear Walls Database

A considerable number of RC squat walls have been tested for the last several decades to understand their behavior and to study the effect of the main variables on peak shear strength. Tests were performed on rectangular walls constructed with and without boundary elements. These were subjected to horizontal and axial loads (see Figure 2). The results of 298 and 189 tests performed on rectangular squat walls constructed with boundary elements (RWBEs) and rectangular walls without boundary elements (RWs), respectively, are used in the development of the ANN and strut and tie models. These are taken from the database assembled by Chetchotisak et al. [23].

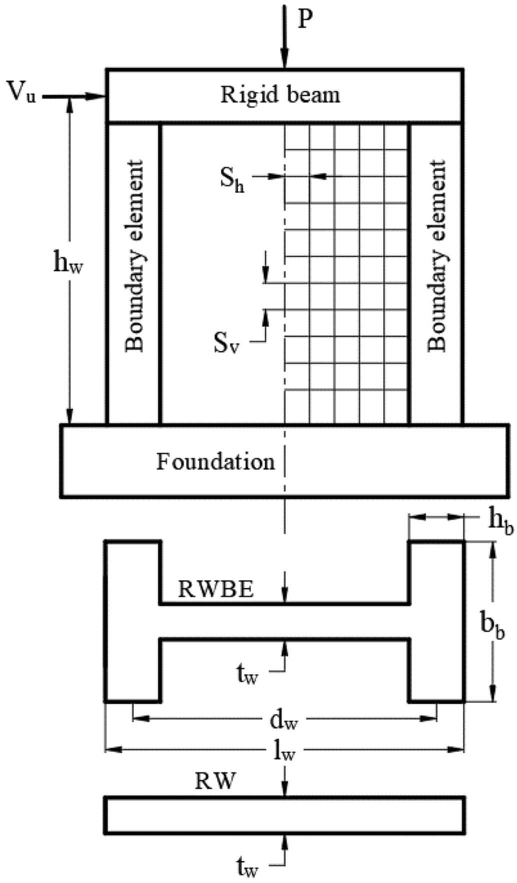

Figure 2. A typical squat wall under vertical and lateral loads

The test results of RWBEs consist of 107 and 191 flanged walls and walls constructed with boundary columns, respectively. While the test results of RWs include 133 walls with vertical boundary reinforcements, and the rest have no vertical boundary reinforcements.

Squat walls utilized in this study were loaded by various types of horizontal loads such as monotonic, dynamic, repeated, and cyclic, and the latter is applied to most of these walls. The database includes squat walls that experienced premature shear failure only, while those experience flexural and sliding failures are left out. Table 1 summarizes the statistical information of the main parameters of the database analyzed in this study, where fc, h_w/l_w, ρ_h, ρ_v, ρ_b, and P/f_cA_w are the concrete compressive strength, the wall's aspect ratio, the horizontal reinforcement ratio, the vertical reinforcement ratio, the vertical boundary reinforcement ratio, and the axial load ratio, respectively. The whole database and the strength predictions are presented in Tables A-1 and A-2 in Appendix I.

Table 1. Statistical information of the main variables

Type	Variables	Statistical parameters				
		Mean	Standard deviation	Minimum	Maximum	Range
RWBEs	f_c (MPa)	38.3	22.7	10.0	111.0	101.0
	h_w/l_w	0.80	0.36	0.28	2.20	1.92
	ρ_h (%)	0.73	0.48	0.00	2.76	2.76
	ρ_v (%)	0.75	0.49	0.00	2.76	2.76
	ρ_b (%)	2.78	1.76	0.44	9.70	9.26
	P/f_cA_w (%)	0.05	0.06	0.00	0.32	0.32
RWs	f_c (MPa)	31.3	9.3	14.0	58.0	44.0
	h_w/l_w	1.06	0.52	0.33	2.17	1.84
	ρ_h (%)	0.60	0.39	0.00	1.59	1.59
	ρ_v (%)	0.75	0.58	0.10	2.87	2.77
	ρ_b (%)	3.06	2.23	0.34	12.75	12.41
	P/f_cA_w (%)	0.03	0.06	0.00	0.40	0.40

3. Artificial Neural Network (ANN)

3.1. Overview

It is a data processing technique operating based on the human nervous system. The structure of this technique consists of numerous processing components (neurons) working jointly to tackle a particular problem. Each neuron transforms a weighted input using the bias and transfer function to output. The advantage of ANN over the other traditional methods is due to the direct application of test data in solving complex problems without prior assumptions, where the solution is obtained through learning by examples like a human [30]. Owing to the ANN's robust process capability, it is now widely used to solve problems in various fields of civil engineering [31, 32].

3.2. Development of ANN Models

Two ANN models are built in the present study: one for RWBEs and the other for RWs. It allows for the fact that peak shear strength produced by the former is higher than that developed by the latter due to the confining effect associated with the presence of boundary elements and the reduction in cracking and concrete strength softening [14, 33]. The architecture of each model consists of an input layer, a hidden layer, and an output layer. The input layer comprises the parameters (pi) employed to predict the shear strength, and the output layer includes the normalized peak shear strength ($v = V_{test}/A_w$). The input parameters are selected according to the previous investigations [14, 17]. It is noted that the number of neurons in the hidden layer is determined using the trial and error method to reach the best correlation with the experimental results, and the use of a large number of neurons in the hidden does not develop the accuracy and sometimes lead to overfitting [30]. The number of neurons in the hidden layer (m) of the RWBEs and RWs models is 21 and 13, respectively. Figure 3 shows the architecture of the above models, where p, w, v, and b denote the input, the weights of hidden and output layers, and the bias, respectively.

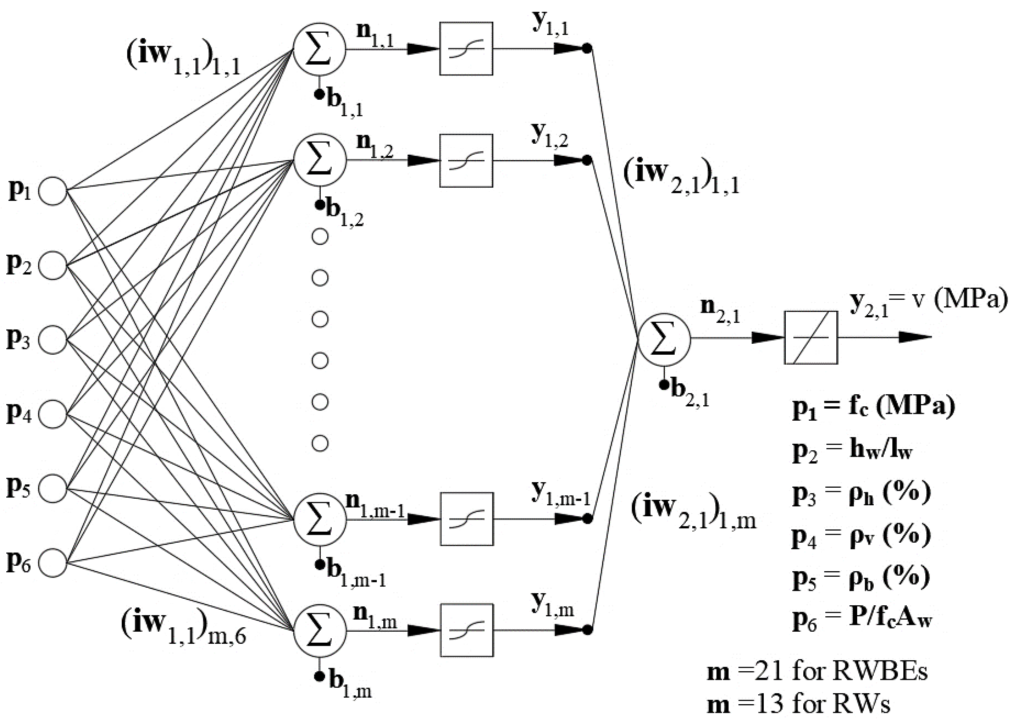

Figure 3. Architecture of the ANN models

The previously described test results are employed to develop the ANN models for RWBEs and RWs and are divided into three parts: 70%, 15%, and 15% for training, testing, and validating the ANN models. The proposed models adopt the Levenberg–Marquardt back-propagation algorithm, and the TANSIG and PURELIN transfer functions are for hidden and output layers. The peak strength is calculated by minimizing the deviation between the ANN predictions and the expected output through back-propagation to the input layer to modify the weights between neurons and biases. This procedure continues until reaching the desired results. In addition, the early stopping technique is utilized to prevent overfitting and maintain the generality of the models [30]. Comparisons between the ANN models and the test results are presented in Figure 4. Furthermore, the performance of the ANN models is measured using the average ratio of estimated-to-measured strength (AVG), the coefficient of variation (COV), and the correlation coefficient (R). The AVG, COV, and R of the RWBEs model are 1.01, 0.10, and 0.98, respectively, and the AVG, COV, and R of the RWs model are 1.00, 0.10, and 0.98, respectively. The statistical analysis confirms that both models correlate well with the available database, as the R of these models is higher than 0.8 [34].

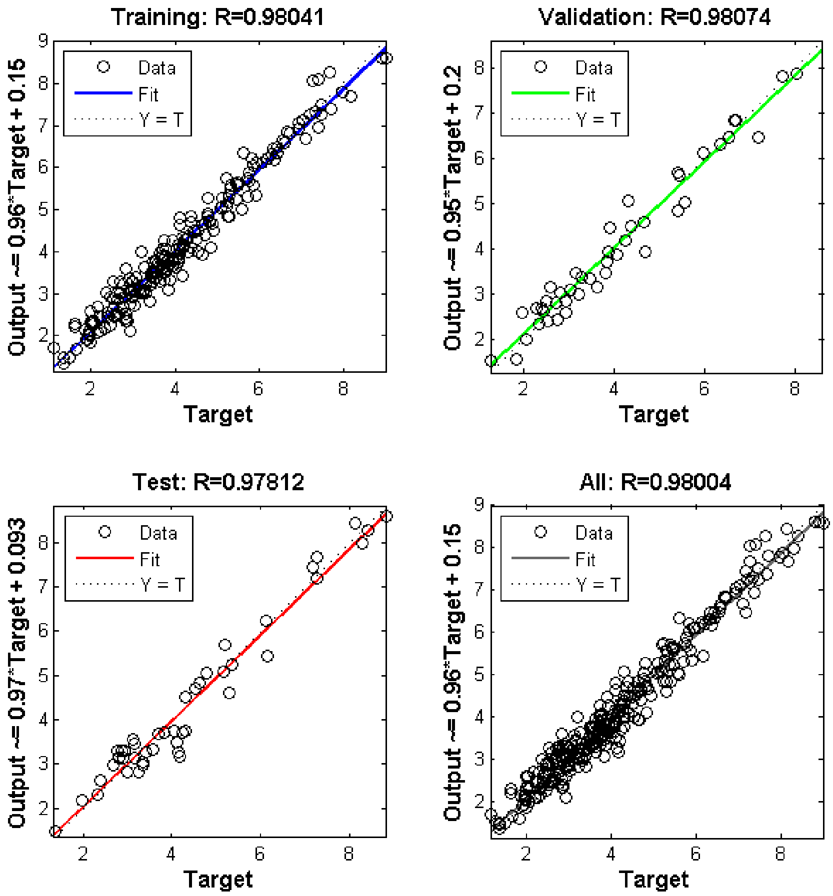

(a) RWBEs

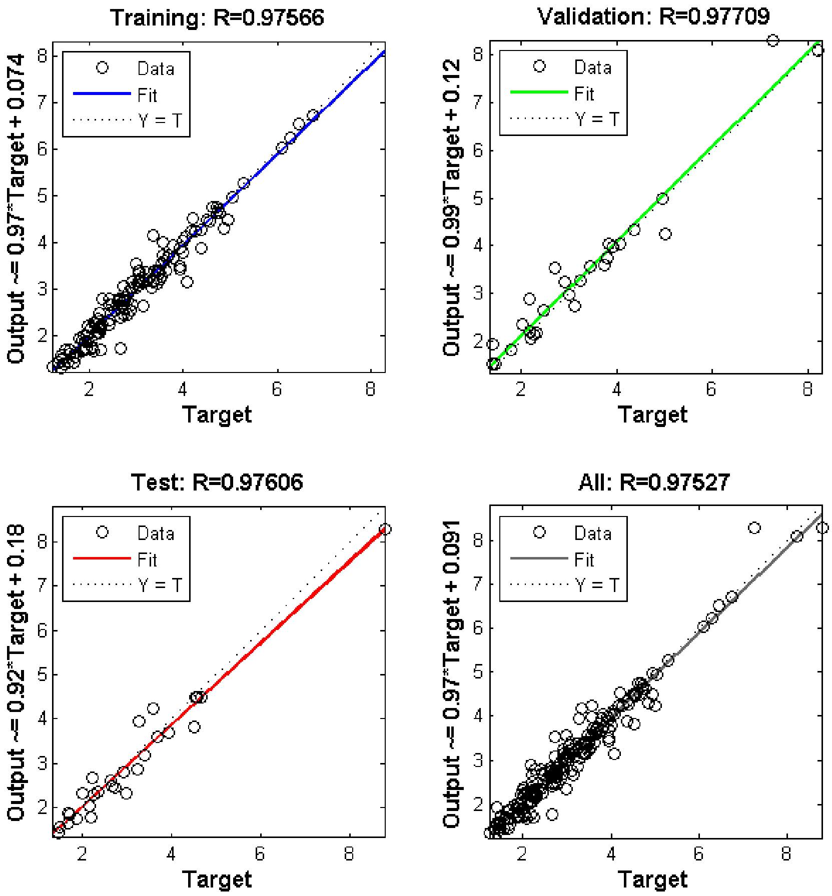

(b) RWs

Figure 4. Performance of the ANN models

3.3. Parametric analysis

Parametric analysis is performed using the ANN models to study the effect of the input parameters on the peak shear strength of RWBEs and RWs. In doing so, the selected ANN input ranges from its smallest value within the database to the highest one and holds the rest inputs at their average values within the database [35]. The average of the ANN inputs set to f_c = 38.3 MPa, h_w/l_w = 0.80, ρ_h = 0.73%, ρ_v = 0.75%, ρ_b = 2.78%, $P/f_c A_w$ = 0.05 in the calculations of the RWBEs strength, and the average of the ANN inputs set to f_c = 31.3 MPa, h_w/l_w = 1.06, ρ_h = 0.60%, ρ_v = 0.75%, ρ_b = 3.06%, $P/f_c A_w$ = 0.03 in the calculations of the RWs strength.

Figure 5-a shows the effect of concrete strength (f_c) on the normalized peak strength ($v = V_{test}/A_w$) of the RWBEs and RWs walls. The shear strength increases with concrete strength, and this trend has been observed experimentally by Gulec and Whittaker [17]. The concrete contribution is acknowledged using square and cubic roots in the ACI-318-19 [36] and EC8 [37].

Figure 5-b demonstrates the influence of the aspect ratio (h_w/l_w) on ($v = V_{test}/A_w$) of the RWBEs and RWs. As inferred from this figure that the shear strength decreases with the increase of this parameter, which is parallel with the previous experimental studies. The influence of h_w/l_w on shear strength is considered in various existing models to allow for the fact that shorter walls reduce the path to transfer the load to supports through a compressive diagonal strut, subsequently leading to concrete crushing at higher load-carrying capacity than that of slender walls.

Figure 5-c displays the predicted (v) with the variation of horizontal reinforcement ratio (ρ_h). It indicates that the shear strength of RWBEs decreases with the increase of ρ_h from 0 to 1.5%. However, it increases with ρ_h from 1.5% to 2.76%. The shear strength of RWs increases with the ρ_h to a specific limit (ρ_h = 1.2%), beyond which the shear strength decreases with the increase of ρ_h. The effect of this parameter is still unclear because some scholars indicated that ρ_h has negligible influence on shear strength [38-40], while others indicated that the influence of ρ_h is modest compared to ρ_v [14, 23]. On the other hand, ACI-318-19 [36] and Baghi et al. [25] point out that this parameter significantly affects the peak shear strength.

Figure 5-d presents the effect of vertical reinforcement ratio (ρ_v) on v. It clearly shows that the shear strength of RWBEs walls when ρ_v increases from 0% to 1.5% and decreases when ρ_v increases from 1.5% to 2.76%. The shear strength of RWs increases with ρ_v increases to a specific limit (ρ_v = 1.5%), beyond which the shear strength decreases with increasing ρ_v. Similar to ρ_h, there remains uncertainty concerning the influence of ρ_v. That is, the ACI-318-19 [36] and Sanchez-Alejandre and Alcocer [16] ignore this parameter in the calculations of shear strength, while others found that the contribution of this parameter to the peak shear strength is higher than that of ρ_h [14, 23].

The peak shear strength of RWBEs and RWs walls with the variation of the boundary elements' vertical reinforcement ratio (ρ_b) is explained in Fig. 5-e, where the shear strength of RWBEs enhances with ρ_b, while that of RWs increase when ρ_b increase from 0.34% to 7.2% and decrease when ρ_b increase from 7.2% to 12.75%. There is no consensus about the role of ρ_b in estimating the peak strength, as some models take into account the effect of ρ_b [17, 23, 25], and others overlook this parameter [15,18, 14, 23, 36].

Fig. 5-f plots the variation of the axial load ratio (P/f_cA_w) against the shear strength of RWBEs and RWs walls. For the RWBEs walls, the strength improves with the (P/f_cA_w) from 0 to 0.16, beyond which declines with increasing (P/f_cA_w). Similarly, the peak strength of RWs develops with (P/f_cA_w) from 0 to 0.2% and descends beyond the latter ratio. This parameter is considered in the majority of the existing models while ignored by ACI-318-19 [36] and EC8 [37].

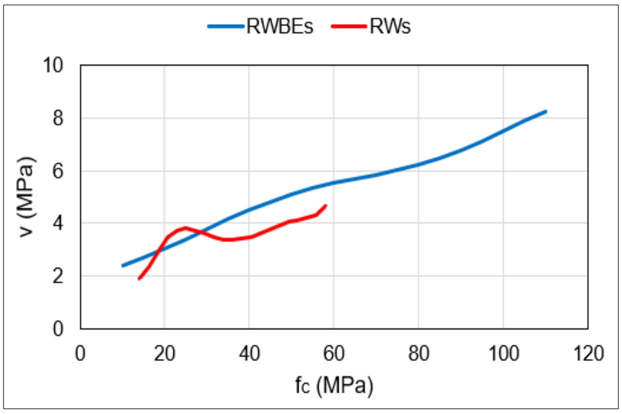

(a) f_c

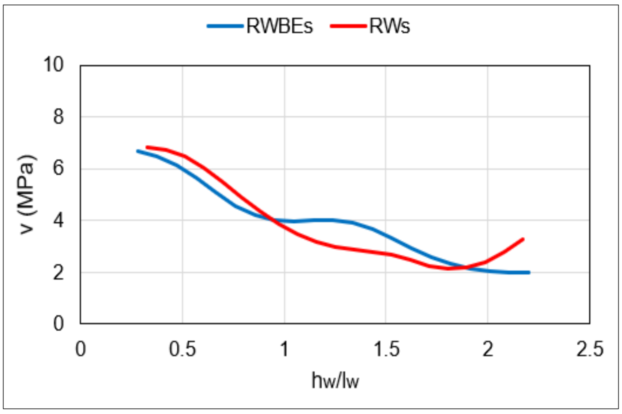

(b) h_w/l_w

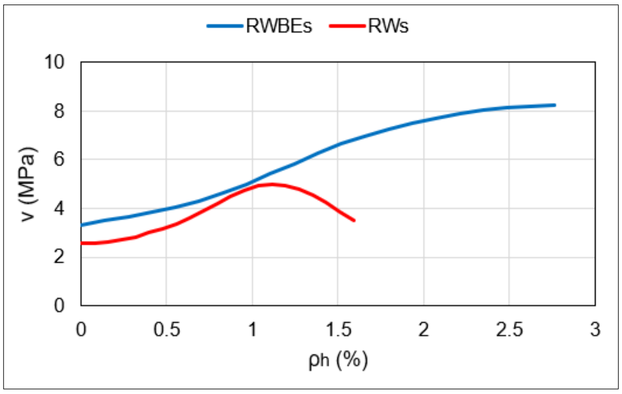

(c) ρ_h

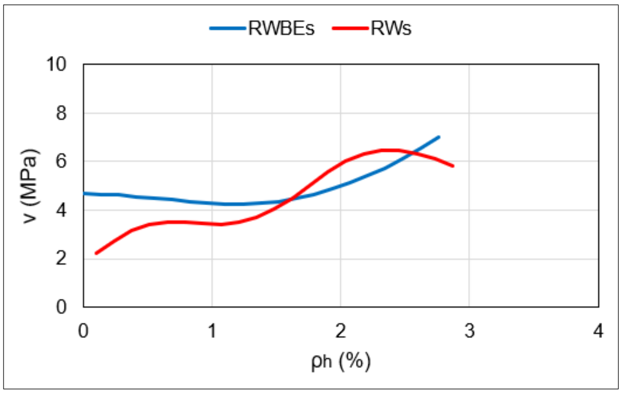

(d) ρ_v

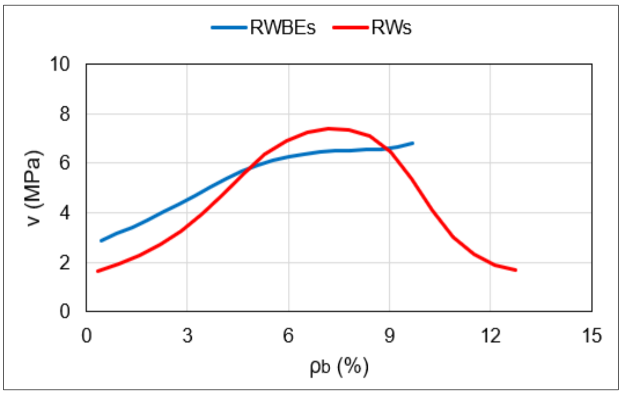

(e) ρ_b

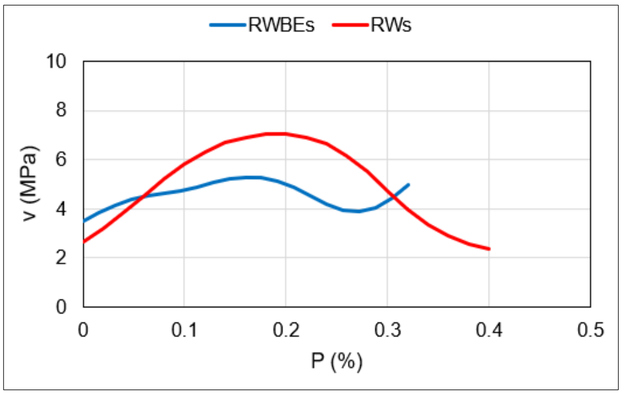

(f) P/f_cA_w

Figure 5. Effect of input parameters

3.4. Sensitivity Analysis

It is carried out to estimate the contribution of the input variables to the ANN peak shear strength. Garson [41] introduced an algorithm to determine the relative importance (RI) of each of the ANN inputs, and the larger value of (RI) indicates a higher contribution to the peak shear strength. A detailed description of the RI calculations can be found elsewhere [30], and below is the summary:

$$P_{ij} = |W_{ij}| \times |W_{i1}| \tag{1}$$

$$Q_{ij} = {P_{ij}}\big/{(P_{i1} + P_{i2} + \cdots + P_{im})} \tag{2}$$

$$S_j = (Q_{1j} + Q_{2j} + \cdots + Q_{kj}) \tag{3}$$

$$RI_1 = {S_1 \times 100}\big/{(S_1 + S_2 + \cdots + S_m)} \tag{4}$$

in which, P_{ij} is a product of the absolute value of the matrixes W_{ij} and W_{i1}, which are the weights of input j in the hidden neuron i, and output neuron 1 in hidden neuron I, respectively; k is Eq. (3) denotes the number of neurons in the hidden layer.

Table 2 presents the RI values of the input parameters of the RWBEs and RWs models. It indicates that the concrete strength is the most significant parameter and the horizontal reinforcement ratio is the least contributing one. It is hardly surprising since the former parameter (f_c) represents the average shear stresses through the section simplifying the complex shear behavior and therefore adopted in every peak strength expression [42], and the influence of the latter (ρ_h) is minor on the peak shear strength [27-29]. It should be noted that the obtained results are comparable to those of Chetchotisak et al. [23].

Table 2. Relative importance and ranking of the input parameters

Type	Parameter	f_c	h_w/l_w	ρ_h	ρ_v	ρ_b	P/f_cA_w
RWBEs	Relative importance	0.22	0.19	0.13	0.17	0.17	0.15
	Ranking	1	2	5	3	3	4
RWs	Relative importance	0.21	0.17	0.13	0.18	0.17	0.15
	Ranking	1	4	6	2	3	5

4. Strut and Tie Model

Because of the geometrical properties of squat walls, they are considered disturbed regions (D-regions) with complex stress trajectories and nonlinear strain distributions. Hence, the strut and tie method is adopted to develop the proposed design as viewed to be an appropriate approach to replicate the load-transferring mechanism of such regions and squat walls [20, 21].

Figure 6 presents a typical squat wall constructed with boundary elements, supported on a rigid foundation and loaded vertically by (P) and laterally by (V_u). It reinforces with vertical and horizontal steel bars uniformly spaced at S_v and S_h, respectively.

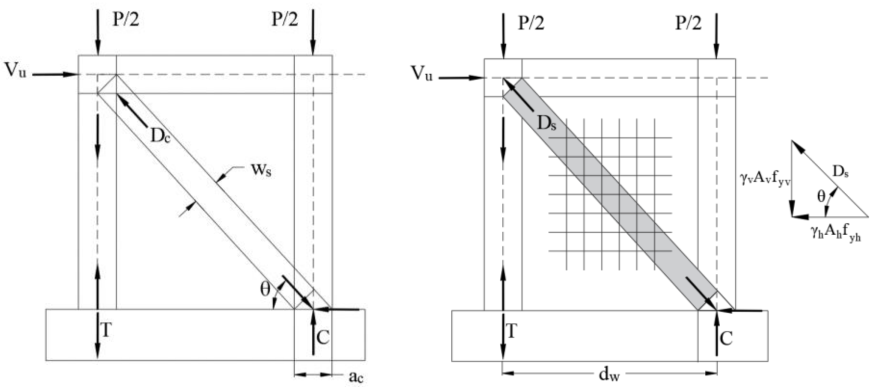

(a) Diagonal strut mechanism (b) Web mechanism

Figure 6. The proposed strut and tie model

The design model assumes that the peak shear strength for squat walls with enough flexural capacity is obtained from the diagonal strut mechanism, V_c, and web reinforcement mechanism, V_w [14, 20, 21, 23]:

$$V_n = V_c + V_w \tag{5}$$

The compressive diagonal strut (D_s) resists the lateral (Vn) and axial load (P/2), where the latter is divided into two concentrated loads acting at the boundary elements (R). For RWBEs, the vertical steel bars of boundary elements withstand the tensile force (T). However, for RWs, it is assumed that the vertical steel bars in an effective width of (0.1 l_w) at both ends of a wall resist the tensile force (T), and the rest of the vertical reinforcement in (0.8 l_w) contribute to the truss mechanism [14, 20, 21, 23].

4.1. Diagonal Strut Mechanism

This mechanism includes the contribution of concrete replicated by a single compressive strut, forming as shown in Figure 6-a and inclined at angle θ. The latter is determined from the wall's aspect ratio and is given by:

$$\theta = \frac{h_w}{d_w} \tag{6}$$

$d_w = l_w - h_b$ is the horizontal length of a wall between the compression and tension forces developed in the boundary elements; h_w, l_w, and h_b are the height of a wall, the length of a wall, and the length of a boundary element, respectively. As previously mentioned, h_b is considered as $0.1 l_w$ for RWs. The equilibrium equations below are obtained from the transferring load mechanism

$$V_c = D_c \cos\theta \tag{7}$$

$$C = T = D_c \sin\theta \tag{8}$$

C and T are the compressive and tension forces developed in the boundary elements. The diagonal strut usually forms in a bottle shape. However, for simplicity, it is considered prismatic with a uniform width. The corresponding cross-section area of the diagonal strut is given by:

$$A_{strut} = w_s t_w \tag{9}$$

w_s and t_w are the width and depth of the diagonal strut. It is widely accepted to assume that w_s equal to the depth of the concrete compression zone of an elastic column [14, 20, 21, 23]. Hence, it is given by:

$$w_s = a_c = \left(0.25 + \frac{0.85 h_c}{A_w f_c}\right) l_w \tag{10}$$

The compressive force of the diagonal strut computes from the product of the cross-section area (A_{strut}) and effective concrete strength (f_{ce}):

$$D_c = f_{ce}A_{strut} \tag{11}$$

The effective compressive strength of the diagonal strut is considered a function of concrete strength and determined from the following equation:

$$f_{ce} = \gamma_c \eta f_c \tag{12}$$

A is an empirical coefficient calibrated using the test results, and η is a softening factor suggested by the fib-Model Code 2010 [43] to design D-regions:

$$\eta = \left(\frac{30}{f_c}\right)^{1/3} \leq 1 \tag{13}$$

By substituting, Equations 10 to 13 into Equation 9, the diagonal strut mechanism takes the following form:

$$V_c = \gamma_c\, \eta f_c A_{strut} \cos\theta \tag{14}$$

4.2. Web Mechanism

In addition to the diagonal strut mechanism, the web mechanism (V_w) developed by the horizontal and vertical reinforcements is a significant strength element because these reinforcements provide an additional load path alongside the diagonal strut and consequently improve the wall peak shear capacity [14, 21, 23,43]. It is proposed that the web reinforcements form a diagonal compression force (D_s) acting on the same line as that provided by concrete, D_c [44, 45]. The strength contribution of the web mechanism (V_w) is equal to Ds, which estimates from the vector sum of the forces developed by the horizontal and vertical reinforcements, see Figure 6-b. Since the current loading situation is very much similar to those in beam-column joints and deep beams [44, 45], the contribution of the web mechanism is expressed as by:

$$V_s = V_h + V_v = \gamma_h A_h f_{yh} + \gamma_v A_v f_{yv} \cot\theta \tag{15}$$

γ_h and γ_v are empirical parameters to be calibrated with the test results to allow for the fact that web reinforcements do not develop their yield strengths [14, 44,45]; A_h and A_v are the area of horizontal and vertical reinforcements, where $A_h = \rho_h h_w t_w$ and $A_v = \rho_v l_w t_w$; f_{yh} and f_{yv} are the yield strength of horizontal and vertical reinforcements; $\rho_h$and ρ_v are the reinforcement ratio of the horizontal and vertical rebars, respectively.

4.3. Peak Shear Strength Expression

When Equations 14 and 15 are substituted in Equations 5, the peak shear expression is given by:

$$V_n = \gamma_c \eta f_c A_{strut} \cos\theta + \gamma_h A_h f_{yh} + \gamma_v A_v f_{yv} \cot\theta \tag{16}$$

The unknown parameters (γ_c, γ_h, and γ_v) are determined from regression analysis using the above-described database. It is worth noting that the database of RWBEs and RWs walls is divided into two sets: one consists of (70%) employed to calibrate the proposed model, and the other set includes the remaining (30%) for validation. In particular, the results of 209 RWBEs and 132 RWs walls are for calibration, and the rest results of 89 RWBEs and 57 of RWs are for validation.

The optimum values of the above parameters are estimated to improve the accuracy and to decrease the coefficient of variation (COV) of the calculated-to-measured strength ratio.

The analysis results in $\gamma_c = 0.64$, $\gamma_h = 0.30$, and $\gamma_v = 0.15$ for RWBEs and $\gamma_c = 0.26$, $\gamma_h = 0.33$, and $\gamma_v = 0.22$ for RWs. By substituting these results into Eq. (16), the peak strength expressions can be expressed as follow:

For RWBEs:

$$V_n = 0.64\eta f_c A_{strut} \cos\theta + 0.30 A_h f_{yh} + 0.15 A_v f_{yv} \cot\theta \tag{17-a}$$

For RWs:

$$V_n = 0.26\eta f_c A_{strut} \cos\theta + 0.33 A_h f_{yh} + 0.22 A_v f_{yv} \cot\theta \tag{17-b}$$

A keen observation of the empirical parameters in Equations 17-a and 17-b indicates that the values of these parameters are higher in the former than those in the latter, reflecting the strength enhancement provided by the confining effect associated with the presence of the boundary elements. In addition, the higher values γ_h in RWBEs and RWs expressions compared to those of γ_v suggest that the strength contribution of the horizontal reinforcement is higher than that provided by the vertical bars. This finding is consistent with the ACI-318-19 [36] and Baghi et al. [25] and significantly different from those of Barda et al. [38], Maier and Thürlimann [39], Lefas et al. [40], Kassem [14], Chetchotisak et al. [23], and the proposed ANN models. Further investigations are needed to clarify such contradictions.

Comparisons with the available database mark the reasonable agreement between the calculated and measured strengths, as presented in Figures 7-a, and 7-b. The AVG is 1.00 and 1.02 for RWBEs using calibration and validation sets, respectively, with COV of 0.19 and 0.16, respectively; while the AVG 1.01 and 1.02 for RWs using calibration and validation sets, with COV of 0.18 and 0.20, respectively. It is noteworthy that the close values of the statistical parameters confirm the generality of the proposed model

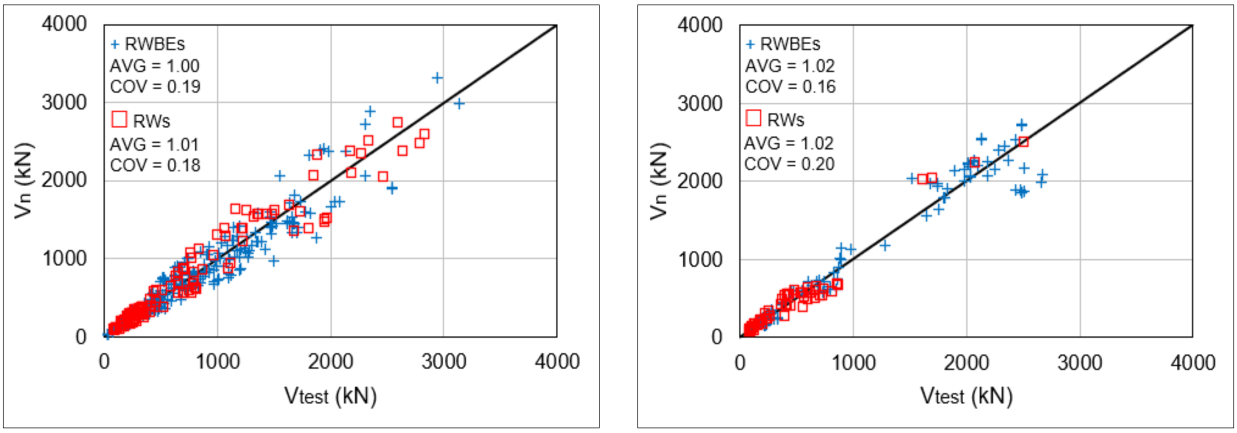

(a) Calibration set (b) Validation set

Figure 7. Performance of the proposed strut and tie model

4.4. Comparisons with Existing Models

To inspect the accuracy of the design model regarding those in existence, the peak strength models of the ACI-318-19 [36], EC8 [37], Wood [15], Hwang & Lee [21], Sanchez-Alejandre & Alcocer [16], Kassem [14], and Baghi et al. [25] are considered and summarized in Table 3.

Table 3. Summary of existing models

Source	Peak Strength expressions
ACI-318-19 [36]	$V_{ACI} = (\alpha_c\sqrt{f_c} + \rho_h f_{yh}) \leq 0.83\sqrt{f_c}A_{cv}$ $\alpha_c = 0.25$ for $\frac{h_w}{l_w} \leq 1.5$, $\alpha_c = 0.17$ for $\frac{h_w}{l_w} > 2.0$, α_c can be determined using linear interpolation for $1.5 < \frac{h_w}{l_w} < 2.0$
EC8 [37]	$V_{Rd} = 0.18k(\rho_v f_c)^{1/3} + 0.75\rho_h f_{yh} b_w l_w,\ k = 1 + \sqrt{\frac{200}{d}} \leq V_{Rdmax} = {}^{b_w z f_c}/_{\tan\theta + \cot\theta}$
Wood [15]	$0.5\sqrt{f_c} \leq V_{Wood} = 0.25A_v f_{yv} \leq 0.83\sqrt{f_c}A_{cv}$
Hwang & Lee [21]	$V_{H\&L} = K\xi f_c A_{str}\cos\theta,\ K = K_h + K_v - 1,$ $\gamma = {}^{3.35}/_{f_c} \leq 0.52\ ,\ A_{str} = \left(0.25 + \frac{0.85h_c}{A_w f_c'}\right) l_w t_w$ K_h & K_v are functions of horizontal and vertical reinforcements
Sanchez-Alejandre & Alcocer [16]	$V_{S\&A} = \left[\left(\gamma\eta_v + 0.04\,{}^{P}/_{A_w}\right)\sqrt{f_c} + \eta_h\rho_h f_{yh}\right] A_w$ $\gamma = 0.42 - 0.08\,{}^{h_w}/_{l_w},\ \eta_v = 0.75 + 0.05\rho_v f_{yv},$ $\eta_h = 1 - 0.16\rho_h f_{yh} \geq 0.20\ MPa$
Kassem [14]	$V_{K-RWBE} = 0.67f_c\left(\psi k_s \sin 2\theta + 0.30\omega_h\,{}^{h_w}/_{l_w} + 1.74\omega_v\cot\theta\right) d_w t_w \leq 1.25\sqrt{f_c}d_w t_w,\ \omega_h = \frac{\rho_h f_{yh}}{f_c}$ $V_{K-RW} = 0.44f_c\left(\psi k_s \sin 2\theta + 0.10\omega_h\,{}^{h_w}/_{l_w} + 0.3\omega_v\cot\theta\right) d_w t_w \leq 1.25\sqrt{f_c}d_w t_w,\ \omega_v = \frac{\rho_v f_{yv}}{f_c}$ $d_w = l_w - {}^{h_b}/_2 - {}^{a_s}/_3,\ a_s = \left(0.25 + \frac{0.85h_c}{A_w f_c}\right) l_w$
Baghi et al. [25]	$V_B = 2\beta f_c^{\,0.65} b_b h_b + \beta f_c^{\,0.65} t_w l_w + \rho_h f_{yh}\cot\theta\, t_w l_w$ $\beta = \alpha(0.2x^{0.02} - 0.1x^{1.5}),\ \theta = 0.6\beta^{-0.8} + 60$ $x = \left(\frac{\rho_b f_{yb}}{f_c} + \frac{\rho_v f_{yv}}{f_c}\right)\frac{h_w}{l_w},\ y = \left(\frac{\rho_h f_{yh}}{f_c} + \frac{P}{A_w f_c}\right)$

Although the proposed model agrees well with the available test results and achieved the least COV compared to the existing models, it is not applicable in practice because 46% of its strength estimations are unsafe (V_n/V_{test}> 1), see Figure 8. Therefore, a reduction factor of 0.75 is suggested based on statistical analysis to multiply by Equation 17 to develop a design expression that produces conservative strength estimations and eliminates undesirable unsafe ones.

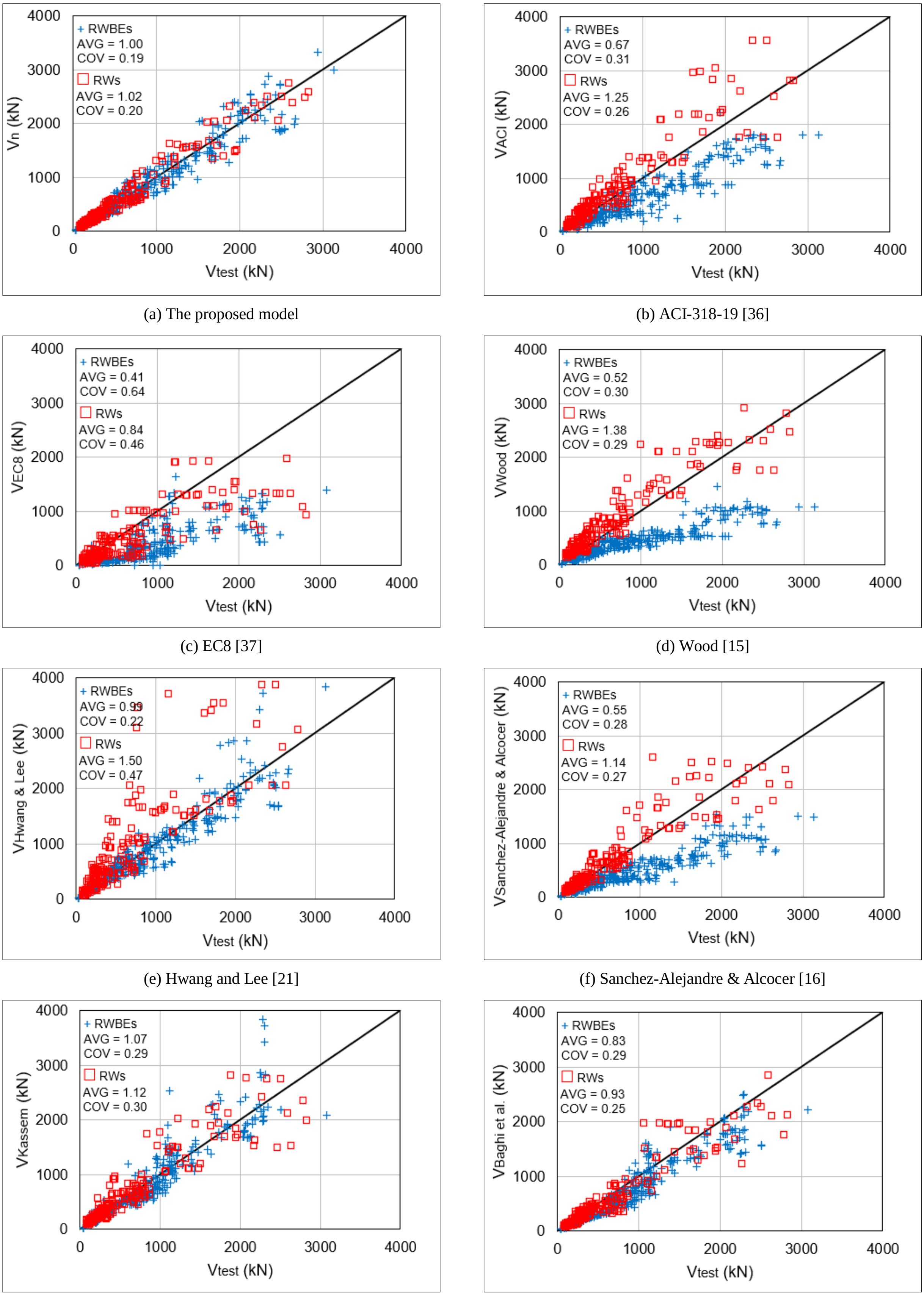

(a) The proposed model (b) ACI-318-19 [36]

(c) EC8 [37] (d) Wood [15]

(e) Hwang and Lee [21] (f) Sanchez-Alejandre & Alcocer [16]

(g) Kassem [14] (h) Baghi et al. [25]

Figure 8. Strength estimations using the proposed and existing models

5. Conclusions

This research has investigated the peak shear strength of squat walls using the ANN technique and the strut and tie method, considering the test results of 487 squat walls that failed in shear with a broad range of test parameters. The findings from the above analysis are summarized below:

- The ANN models have provided the best correlation with the considered database compared to the proposed strut and tie model and those in existence. The AVG, COV, and R of the RWBEs model are 1.01, 0.10, and 0.98, respectively. The corresponding values of the RWs model are 1.00, 0.10, and 0.98, respectively.
- The ANN parametric analysis suggests that the normalized peak shear strength of the RWBEs walls increases with the concrete strength, vertical and horizontal reinforcement ratios, vertical reinforcement in boundary elements, and decreases with the wall aspect ratio. Also, the analysis indicates that the normalized strength of RWs increases with concrete strength and vertical reinforcement ratio while declining with aspect ratio. The normalized strength of the RWs walls improves by increasing the horizontal and vertical reinforcement ratios and the vertical reinforcement ratio of boundary elements to a specific limit, beyond which it decreases. Similarly, the normalized strength of RWBEs and RWs enhances with the axial load ratio to a definite limit and then further descends.
- The sensitivity analysis using the Garson algorithm suggests that the concrete strength is the highest contributing input to the normalized peak shear strength of the RWBEs and RWs, while the horizontal reinforcement provides the lowest contribution.
- The proposed softened strut and tie model provides improved correlations with the test results than the existing models because of the considered parameters and the wide-ranging database.

6. Declarations

6.1. Data Availability Statement

The data presented in this study are available in the article.

6.2. Funding

The author received no financial support for the research, authorship, and/or publication of this article.

6.3. Conflicts of Interest

The author declares no conflict of interest.

7. References

[1] Paulay, T., & Priestley, M. N. (1992). Seismic design of reinforced concrete and masonry buildings (Vol. 768). Wiley, New York, United States. doi:10.1002/9780470172841.

[2] Terzioglu, T., Orakcal, K., & Massone, L. M. (2018). Cyclic lateral load behavior of squat reinforced concrete walls. Engineering Structures, 160, 147–160. doi:10.1016/j.engstruct.2018.01.024.

[3] Gulec, C. K., & Whittaker, A. S. (2009). Performance-based assessment and design of squat reinforced concrete shear walls. Technical Report MCEER-09-0010, State University of New York, Buffalo, United States.

[4] Cortés-Puentes, W. L., & Palermo, D. (2018). Performance of pre-1970s squat reinforced concrete shear walls. Canadian Journal of Civil Engineering, 45(11), 922–935. doi:10.1139/cjce-2017-0595.

[5] Gulec, C. K., Whittaker, A. S., & Stojadinovic, B. (2008). Shear strength of squat rectangular reinforced concrete walls. ACI Structural Journal, 105(4), 488–497. doi:10.14359/19863.

[6] Benjamin, J. R., & Williams, H. A. (1957). The Behavior of One-Story Reinforced Concrete Shear Walls. Journal of the Structural Division, 83(3). doi:10.1061/jsdeag.0000118.

[7] Cardenas, A. E., Hanson, J. M., Corley, W. G., & Hognestad, E. (1973). Design provisions for shear walls. ACI Journal, 70(3), 221-230. doi:10.14359/11201.

[8] Paulay, T., Priestley, M. J. N., & Synge, A. J. (1982). Ductility in Earthquake Resisting Squat Shear walls. Journal of the American Concrete Institute, 79(4), 257–269. doi:10.14359/10903.

[9] Shaingchin, S., Lukkunaprasit, P., & Wood, S. L. (2007). Influence of diagonal web reinforcement on cyclic behavior of structural walls. Engineering Structures, 29(4), 498–510. doi:10.1016/j.engstruct.2006.05.016.

[10] Cheng, M. Y., Wibowo, L. S. B., Giduquio, M. B., & Lequesne, R. D. (2021). Strength and deformation of reinforced concrete squat walls with high-strength materials. ACI Structural Journal, 118(1), 125–137. doi:10.14359/51728082.

[11] Kim, J. H., & Park, H. G. (2022). Shear Strength of Flanged Squat Walls with 690 MPa Reinforcing Bars. ACI Structural Journal, 119(2), 209–220. doi:10.14359/51734142.

[12] Chandra, J., Chanthabouala, K., & Teng, S. (2018). Truss model for shear strength of structural concrete walls. ACI Structural Journal, 115(2), 323–335. doi:10.14359/51701129.

[13] Sivaguru, V., & Rao, G. A. (2021). Strength and behavior of reinforced concrete squat shear walls with openings under cyclic loading. ACI Structural Journal, 118(5), 235–250. doi:10.14359/51732832.

[14] Kassem, W. (2015). Shear strength of squat walls: A strut-and-tie model and closed-form design formula. Engineering Structures, 84, 430–438. doi:10.1016/j.engstruct.2014.11.027.

[15] Wood, S. L. (1990). Shear strength of low-rise reinforced concrete walls. Structural Journal, 87(1), 99-107. doi:10.14359/2951.

[16] Snchez-Alejandre, A., & Alcocer, S. M. (2010). Shear strength of squat reinforced concrete walls subjected to earthquake loading trends and models. Engineering Structures, 32(8), 2466–2476. doi:10.1016/j.engstruct.2010.04.022.

[17] Gulec, C. K., & Whittaker, A. S. (2011). Empirical Equations for Peak Shear Strength of Low Aspect Ratio Reinforced Concrete Walls. ACI Structural Journal, 108(1), 80-89. doi:10.14359/51664205.

[18] Hsu, T. T. C., & Mo, Y. L. (1985). Softening of Concrete in Low-Rise Shear walls. Journal of the American Concrete Institute, 82(6), 883–889. doi:10.14359/10410.

[19] Massone, L. M., & Melo, F. (2018). General solution for shear strength estimate of RC elements based on panel response. Engineering Structures, 172, 239–252. doi:10.1016/j.engstruct.2018.06.038.

[20] Hwang, S.-J., Fang, W.-H., Lee, H.-J., & Yu, H.-W. (2001). Analytical Model for Predicting Shear Strength of Squat Walls. Journal of Structural Engineering, 127(1), 43–50. doi:10.1061/(asce)0733-9445(2001)127:1(43).

[21] Hwang, S.-J., & Lee, H.-J. (2002). Strength Prediction for Discontinuity Regions by Softened Strut-and-Tie Model. Journal of Structural Engineering, 128(12), 1519–1526. doi:10.1061/(asce)0733-9445(2002)128:12(1519).

[22] Ma, J. X., Chen, K. Y., Wang, Y. H., & Li, B. (2021). Peak shear strength of J-shaped reinforced concrete squat walls. Gongcheng Lixue/Engineering Mechanics, 38(4), 123–135. doi:10.6052/j.issn.1000-4750.2020.05.0337.

[23] Chetchotisak, P., Chomchaipol, W., Teerawong, J., & Shaingchin, S. (2022). Strut-and-tie model for predicting shear strength of squat shear walls under earthquake loads. Engineering Structures, 256, 114042. doi:10.1016/j.engstruct.2022.114042.

[24] Chen, X. L., Fu, J. P., Yao, J. L., & Gan, J. F. (2018). Prediction of shear strength for squat RC walls using a hybrid ANN–PSO model. Engineering with Computers, 34(2), 367–383. doi:10.1007/s00366-017-0547-5.

[25] Baghi, H., Baghi, H., & Siavashi, S. (2019). Novel empirical expression to predict shear strength of reinforced concrete walls based on particle swarm optimization. ACI Structural Journal, 116(5), 247–260. doi:10.14359/51716773.

[26] Gondia, A., Ezzeldin, M., & El-Dakhakhni, W. (2020). Mechanics-Guided Genetic Programming Expression for Shear-Strength Prediction of Squat Reinforced Concrete Walls with Boundary Elements. Journal of Structural Engineering, 146(11), 4020223. doi:10.1061/(asce)st.1943-541x.0002734.

[27] Tariq, M., Khan, A., Ullah, A., Zamin, B., Kashyzadeh, K. R., & Ahmad, M. (2022). Gene Expression Programming for Estimating Shear Strength of RC Squat Wall. Buildings, 12(7), 918. doi:10.3390/buildings12070918.

[28] Feng, D.-C., Wang, W.-J., Mangalathu, S., & Taciroglu, E. (2021). Interpretable XGBoost-SHAP Machine-Learning Model for Shear Strength Prediction of Squat RC Walls. Journal of Structural Engineering, 147(11), 4021173. doi:10.1061/(asce)st.1943-541x.0003115.

[29] Parsa, P., & Naderpour, H. (2021). Shear strength estimation of reinforced concrete walls using support vector regression improved by Teaching–learning-based optimization, Particle Swarm optimization, and Harris Hawks Optimization algorithms. Journal of Building Engineering, 44, 102593. doi:10.1016/j.jobe.2021.102593.

[30] Beale, M. H., Hagan, M. T., & Demuth, H. B. (2010). Neural network toolbox. User's Guide, MathWorks, Three Apple Hill Drive Natick, United States.

[31] Onyelowe, K. C., Gnananandarao, T., Ebid, A. M., Mahdi, H. A., Razzaghian Ghadikolaee, M., & Al-Ajamee, M. (2022). Evaluating the Compressive Strength of Recycled Aggregate Concrete Using Novel Artificial Neural Network. Civil Engineering Journal, 8(8), 1679–1693. doi:10.28991/CEJ-2022-08-08-011.

[32] Al-Rawashdeh, M., Yousef, I., & Al-Nawaiseh, M. (2022). Predicting the Inelastic Response of Base Isolated Structures Utilizing Regression Analysis and Artificial Neural Network. Civil Engineering Journal, 8(6), 1178–1193. doi:10.28991/CEJ-2022-08-06-07.

[33] Mansour, M. Y., Dicleli, M., & Lee, J. Y. (2004). Nonlinear Analysis of R/C Low-Rise Shear Walls. Advances in Structural Engineering, 7(4), 345–361. doi:10.1260/1369433041653525.

[34] Smith, G. N. (1986). Probability and statistics in civil engineering. Collins professional and technical books, New York, United States.

[35] Safiee, N. A., & Ashour, A. (2017). Prediction of punching shear capacity of RC flat slabs using artificial neural network. Asian Journal of Civil Engineering, 18(2), 285–309.

[36] ACI 318-19. (2019). Building Code Requirements for Structural Concrete. American Concrete Institute, Farmington Hills, United States.

[37] EN1998-1. (2004). Design for earthquake resistance, Part 1: general rules, seismic actions and rules for buildings. European Committee for Standardization (CEN), Brussels, Belgium.

[38] Barda, F. (1972). Shear strength of low-rise walls with boundary elements. Ph.D. Thesis, Lehigh University, Bethlehem, United States.

[39] Maier, J., & Thürlimann, B. (1985). Fracture tests on reinforced concrete discs. Report/Institute for Structural Analysis and Construction ETH Zurich, Zurich, Switzerland. (In German). doi:10.1007/978-3-0348-5190-9.

[40] Lefas, I. D., & Kotsovos, M. D. (1990). Strength and deformation characteristics of reinforced concrete walls under load reversals. ACI Structural Journal, 87(6), 716–726. doi:10.14359/2994.

[41] Garson, G. D. (1991). Interpreting neural-network connection weights. AI Expert, 6(4), 46-51.

[42] Krolicki, J., Maffei, J., & Calvi, G. M. (2011). Shear Strength of Reinforced Concrete Walls Subjected to Cyclic Loading. Journal of Earthquake Engineering, 15(sup1), 30–71. doi:10.1080/13632469.2011.562049.

[43] Model Code 2010. (2010). Fib Bulletin 65/66. Federation Internationale Du Beton. Lausanne, Switzerland.

[44] Pauletta, M., Di Luca, D., & Russo, G. (2015). Exterior beam column joints - Shear strength model and design formula. Engineering Structures, 94, 70–81. doi:10.1016/j.engstruct.2015.03.040.

[45] Russo, G., Venir, R., & Pauletta, M. (2005). Reinforced concrete deep beams - Shear strength model and design formula. ACI Structural Journal, 102(3), 429–437. doi:10.14359/14414.

Appendix I

Table A- 1. Test result of RWBEs

No.	Specimen Name	h_w	l_w	t_w	b_b	h_b	ρ_h	ρ_v	ρ_b
1	WAS	2760	2000	80	200	200	0.4	0.4	3.81
2	WBS	3520	2000	80	200	200	0.4	0.4	3.81
3	5	925	1804.4	51	191	127	0.25	0.25	2.09
4	6	925	1804.4	51	191	127	0.25	0.25	2.09
5	7	925	1804.4	51	191	127	0.25	0.25	4.71
6	8	925	1804.4	51	191	127	0.25	0.25	4.71
7	9	925	1804.4	51	191	127	0.25	0.25	4.71
8	10	925	1804.4	51	191	127	0.25	0.25	4.71
9	12	925	1804.4	51	191	127	0.25	0.25	2.09
10	13	925	1804.4	51	191	127	0.5	0.5	2.09
11	14	925	1804.4	51	191	127	0.5	0.5	2.09
12	25	925	1804.4	51	191	127	0.5	0.5	2.09
13	32	925	1804.4	51	191	127	0.5	0.5	2.09
14	33	925	1804.4	51	191	127	0.5	0.5	2.09
15	35	925	1804.4	51	191	127	0.5	0.5	2.09
16	36	925	1804.4	51	191	127	0.5	0.5	2.09
17	37	925	1804.4	51	191	127	0.5	0.5	2.09
18	40	925	1804.4	51	191	127	0.5	0.5	4.71
19	41	925	1804.4	51	191	127	0.5	0.5	4.71
20	43	925	1804.4	51	191	127	0.5	0.5	4.71
21	44	925	1804.4	51	191	127	0.5	0.5	4.71
22	45	925	1804.4	76	191	127	0.25	0.25	2.09
23	46	925	1804.4	76	191	127	0.25	0.25	2.09
24	47	925	1804.4	76	191	127	0.25	0.25	2.09
25	48	925	1804.4	76	191	127	0.25	0.25	2.09
26	49	925	1804.4	76	191	127	0.25	0.25	2.09
27	50	925	1804.4	76	191	127	0.5	0.5	2.09
28	51	925	1804.4	76	191	127	0.5	0.5	2.09
29	52	925	1804.4	76	191	127	0.5	0.5	2.09
30	53	925	1804.4	76	191	127	0.5	0.5	2.09
31	54	925	1804.4	76	191	127	0.5	0.5	2.09
32	56	925	3329.5	51	191	127	0.5	0.5	2.09
33	57	925	3329.5	51	191	127	0.5	0.5	2.09
34	59	925	3329.5	51	191	127	0.5	0.5	2.09
35	B3-2	953	1905	102	610	102	0.48	0.5	4.09
36	B4-3	953	1905	102	610	102	0	0.5	4.09
37	B6-4	953	1905	102	610	102	0.48	0.26	4.09
38	B8-5	1905	1905	102	610	102	0.5	0.5	4.09
39	4BII-1	560	610	50	130	100	0.5	0.5	2.25
40	3A2-3	560	910	50	130	100	0.5	0.5	2.25
41	4BII-3	560	1220	50	130	100	0.5	0.5	2.25
42	BB	2159	2032	203	305	305	0.82	0.82	3.68
43	CW-0.6-1.2-20	1200	2300	80	300	300	1.2	1.2	1.44
44	CW-0.6-0.6-20	1200	2300	80	300	300	0.6	0.6	1.76
45	CW-0.6-0.8-20	1200	2300	80	300	300	0.8	0.8	1.04
46	CW-0.6-1.6-20	1200	2300	80	300	300	1.6	1.6	1.04
47	CW-0.6-2.0-20	1200	2300	80	300	300	2	2	1.04
48	CW-0.6-1.2-40	1200	2300	80	300	300	1.2	1.2	1.04
49	CW-0.4-1.2-20	800	2300	80	300	300	1.2	1.2	1.04
50	CW-0.8-1.2-20	1600	2300	80	300	300	1.2	1.2	1.04
51	CW-0.6-0.6-20a	1200	2300	80	300	300	0.6	0.6	1.04

52	CW-0.6-0.8-20a	1200	2300	80	300	300	0.8	0.8	1.04
53	W7101	1875	2250	80	250	250	0.71	0.71	0.81
54	W7102	1875	2250	80	250	250	0.24	0.24	0.81
55	W7402	1875	2250	80	250	250	0.24	0.24	1.63
56	W7404	1875	2250	80	250	250	0.24	0.24	1.63
57	W7501	1875	2250	80	250	250	0.24	0.24	2.44
58	W7503	1875	2250	80	250	250	0.24	0.24	2.44
59	W7601	1875	2250	80	250	250	0.71	0.71	1.63
60	W7602	1875	2250	100	250	250	0.23	0.23	2.44
61	W7603	1875	2250	100	250	250	0.71	0.71	2.44
62	W7604	2875	2250	80	250	250	0.24	0.24	2.24
63	W7605	2875	2250	100	250	250	0.23	0.23	2.24
64	W7606	1875	2250	100	250	250	0.23	0.23	1.23
65	J1	1200	1000	100	500	120	0.28	0.28	3.88
66	J4	1200	1000	100	120	280	0.28	0.28	6.93
67	J5	2200	1000	100	500	120	0.28	0.28	3.88
68	J6	2200	1000	100	500	120	0.28	0.75	3.88
69	J7	2200	1000	100	500	120	0.75	0.28	3.88
70	CW-0.6-0-20	1200	2300	80	300	300	0	0	1.76
71	CW-0.6-0.3-20	1200	2300	80	300	300	0.3	0.3	1.04
72	CW-0.6-2.4-20	1200	2300	80	300	300	2.36	2.36	1.04
73	CW-0.6-2.8-20	1200	2300	80	300	300	2.76	2.76	1.04
74	CW-0.6-0-0	1200	2300	80	300	300	0	0	1.04
75	CW-0.6-0-40	1200	2300	80	300	300	0	0	1.04
76	CW-0.6-0.6-0	1200	2300	80	300	300	0.6	0.6	1.04
77	CW-0.6-0.6-40	1200	2300	80	300	300	0.6	0.6	1.76
78	CW-0.4-0.6-20	800	2300	80	300	300	0.6	0.6	1.76
79	CW-0.8-0.6-20	1600	2300	80	300	300	0.6	0.6	1.76
80	CW-0.4-2.0-20	800	2300	80	300	300	2	2	1.76
81	CW-0.8-2.0-20	1600	2300	80	300	300	2	2	1.04
82	CW-0.6-2-0	1200	2300	80	300	300	2	2	1.04
83	CW-0.6-2-40	1200	2300	80	300	300	2	2	1.04
84	CW-0.6-2-20B	1200	2300	80	300	300	2	2	1.76
85	CW-0.6-0.6-20L	1200	2300	80	300	300	0.6	0.6	1.04
86	CW-0.6-1.2-20L	1200	2300	80	300	300	1.2	1.2	1.04
87	CW-0.6-2-20L	1200	2300	80	300	300	2	2	1.04
88	Kabeyasawa-K7	1501.14	1998.98	120	200	200	0.53	0.53	1.43
89	Taga-No 1	1200	2180	80	180	180	1.2	1.2	2.89
90	Taga-No 2	1200	2180	80	180	180	1.2	1.2	2.89
91	Taga-No 3	1200	2180	80	180	180	1.2	1.2	2.89
92	Taga-No 4	1200	2180	80	180	180	0.6	0.6	2.89
93	Taga-No 5	1200	2180	80	180	180	2	2	2.89
94	Taga-No 6	1200	2180	80	180	180	2	2	2.89
95	Taga-No 7	1200	2180	80	180	180	2	2	2.89
96	S-1	1100	1000	75	375	100	0.52	0.7	2.1
97	S-2	1100	1000	75	375	100	0.52	0.7	3.04
98	S-3	1100	1000	75	375	100	0.52	0.7	3.87
99	S-4	1100	1000	75	375	100	0.52	1.19	3.15
100	S-5	1100	1000	75	375	100	0.52	1.19	3.99
101	S-6	1100	1000	75	375	100	0.52	1.19	4.46
102	S-7	1100	1000	75	375	100	1.06	0.7	3.04
103	S-F	1100	1000	75	375	100	0.52	0.7	0.84
104	Aoyagi_1-1-148	1520	2720.34	80	320	320	0.76	0.71	1.74
105	Aoyagi_1-2-149	1520	2720.34	80	320	320	0.76	0.71	1.74
106	Aoyagi_1-3-150	1520	2720.34	160	320	320	0.62	0.58	1.74
107	Aoyagi_1-4-151	1520	2720.34	80	320	320	0.76	0.71	6.48

108	Aoyagi_1-5-152	1520	2720.34	160	320	320	0.62	0.58	6.48
109	Endo-1	1750.06	2250.44	80	250	250	0.47	0.49	0.81
110	Endo-2	1750.06	2250.44	80	250	250	0.14	0.16	0.81
111	Endo-3	1750.06	2250.44	80	250	250	0.14	0.16	0.81
112	Endo-4	1750.06	2250.44	50	250	250	0.22	0.26	0.81
113	Endo-5	749.3	2250.44	50	250	250	0.76	0.79	0.81
114	Ryo_1-1-29	1198.88	2300	78	250	250	0.18	0.18	2.55
115	Ryo_1-2-30	1198.88	2300	75	250	250	0.19	0.19	2.54
116	Ryo_2-1-32	1198.88	1550	80	250	250	0.18	0.19	3.21
117	Ryo_2-3-34	1198.88	1550	80	250	250	0.18	0.19	2.55
118	70	1325	2301.24	74	250	250	0.18	0.18	2.54
119	Sugano-71	1325	2301.24	83	250	250	0.07	0.07	2.54
120	Sugano-140	1620	3959.86	120	360	360	0.66	0.66	1.77
121	Sugano-141	1620	3959.86	120	360	360	0.66	0.66	1.77
122	Sugano-142	1620	3959.86	120	360	360	0.66	0.66	1.77
123	Sugano-143	1620	3959.86	120	360	360	0.33	0.33	1.77
124	Sugano-144	1620	3959.86	120	360	360	0.33	0.33	1.77
125	Sugano-145	1620	3959.86	120	360	360	0.66	0.69	1.77
126	Sugano-146	1620	3959.86	120	360	360	0.66	0.69	1.77
127	Sugano-147	1620	3959.86	120	360	360	0.74	0.77	1.77
128	Tsuboi-131	899.16	508	67	120	120	1.89	1.97	8.27
129	Tsuboi-133	899.16	508	67	120	120	2.58	2.53	8.27
130	Tsuboi-134	406.4	508	67	120	120	1.89	1.97	3.95
131	Tsuboi-135	406.4	508	67	120	120	1.89	1.97	8.27
132	W1	2150	1500	100	250	250	0.52	0.39	2.29
133	W2	2150	1500	100	250	250	0.79	0.52	2.29
134	W3	2150	1500	100	250	250	0.74	0.74	2.29
135	W4	2150	1500	100	250	250	1.12	1.12	2.29
136	Ohono_2-1	400	900	70	100	100	0.5	0.1	5
137	Ohono_2-2	400	900	70	100	100	0.5	0.1	5
138	Ohono_2-3	400	900	40	100	100	1	0.2	5
139	Ohono_2-4	400	900	40	100	100	1	0.2	5
140	Ohono_2-5	400	900	40	100	100	0.2	1	5
141	Ohono_2-6	400	900	40	100	100	0.2	1	5
142	NW-2	2261	1700	80	200	200	0.25	0.65	2.14
143	No.1	2261	1700	80	200	200	0.2	0.2	5.08
144	No.2	2261	1700	80	200	200	0.35	0.35	5.08
145	No.3	2261	1700	80	200	200	0.53	0.53	5.08
146	No.4	2261	1700	80	200	200	0.53	0.53	5.08
147	No.6	2261	1700	80	200	200	0.66	0.66	5.08
148	No.7	2261	1700	80	200	200	1	1	5.08
149	No.8	2261	1700	80	200	200	1.45	1.45	5.08
150	DHSCW-01	1900	1000	100	200	200	1.01	1.01	3.39
151	DHSCW-02	1900	1000	100	200	200	1.01	1.01	3.39
152	DHSCW-03	1300	1000	100	200	200	1.01	1.01	3.39
153	DHSCW-04	1300	1000	100	200	200	1.01	1.01	3.39
154	DHSCW-05	800	1000	100	200	200	1.01	1.01	3.39
155	DHSCW-06	800	1000	100	200	200	1.01	1.01	3.39
156	HP0D0	1200	1500	100	1500	100	0.71	0.97	1.26
157	HP5D0	1200	1500	100	1500	100	0.71	0.97	1.26
158	S1	1199	1181	100	400	100	1.01	1.13	1.13
159	S2	1199	1181	100	400	100	1.03	1.16	1.13
160	S3	1199	1181	100	400	100	1.03	2.46	2.55
161	S5	1199	1181.1	100	400	100	1.01	1.13	1.13
162	S6	1199	1181.1	100	400	100	0.57	1.13	1.13
163	S7	1199	1181.1	100	400	100	1.01	1.13	1.13

164	W1	600	1000	60	200	100	0.63	0.63	3.14
165	W2	600	1000	60	200	100	0.55	0.55	3.14
166	W3	600	1000	60	200	100	0.55	0.55	3.14
167	W4	600	1000	60	200	100	0.62	0.62	3.14
168	W5	600	1000	60	200	100	0.31	0.31	3.14
169	S4	1750	1500	200	300	200	0.51	0.54	9.62
170	S4	1750	1500	200	300	200	0.51	0.54	9.7
171	HN4-1	650	860	70	170	80	0.81	0.52	2.09
172	HN4-2	650	860	70	170	80	0.81	0.52	2.09
173	HN4-3	650	860	70	170	80	0.81	0.52	2.09
174	HN6-1	650	860	70	170	80	0.81	0.52	2.09
175	HN6-2	650	860	70	170	80	0.81	0.52	2.09
176	HM4-1	650	860	70	170	80	0.81	0.52	2.09
177	HM4-2	650	860	70	170	80	0.81	0.52	2.09
178	HM4-3	650	860	70	170	80	0.81	0.52	2.09
179	LN4-1	650	860	70	170	80	0.81	0.52	2.09
180	LN4-2	650	860	70	170	80	0.81	0.52	2.09
181	LN4-3	650	860	70	170	80	0.81	0.52	2.09
182	LN6-1	650	860	70	170	80	0.81	0.52	2.09
183	H-HZ4	425	400	30	130	50	0.31	0.48	7.8
184	H-HZ6	425	400	30	130	50	0.31	0.48	7.8
185	H-HZ8	425	400	30	130	50	0.31	0.48	7.8
186	H-HZ10	425	400	30	130	50	0.31	0.48	7.8
187	L-C	900	1200	170	250	250	0.46	0.46	1.65
188	L-M	900	1200	170	250	250	0.46	0.46	1.65
189	M-C	900	1200	170	250	250	0.46	0.46	1.65
190	M-V	900	1200	170	250	250	0.92	0.92	1.65
191	M-H	900	1200	170	250	250	0.46	0.46	1.65
192	U-1	2020	3100	75	2980	100	1.2	1.2	0.44
193	U-2	2019.3	3100	75	2980	100	1.2	1.2	0.44
194	RA-00P	1800	3075	75	1500	75	1.2	1.2	1.23
195	RA-15P	1800	3075	75	1500	75	1.2	1.2	1.23
196	RB-00P	2400	3075	75	1500	75	1.2	1.2	1.23
197	RB-15P	2400	3075	75	1500	75	1.2	1.2	1.23
198	RC-00P	3000	3075	75	1500	75	1.2	1.2	1.23
199	RC-15P	3000	3075	75	1500	75	1.2	1.2	1.23
200	SW1	1100	1000	75	375	100	0.45	0.47	6.43
201	SW2	1100	1000	75	375	100	1.34	1.34	6.43
202	SW3	1100	1000	75	375	100	0.75	0.84	6.43
203	SW4	1100	1000	75	375	100	0.75	0.84	6.43
204	SW5	1100	1000	75	375	100	0.45	1.34	6.43
205	SW6	1100	1000	75	375	100	0.94	1.01	4.25
206	Type N	2050	2050	80	250	250	0.25	0.25	1.81
207	Type S	2050	2050	80	250	250	0.25	0.25	1.81
208	Matui_1-3	880	1000	30	80	80	0.44	0.44	3.8
209	Matui_1-4	880	1000	30	80	80	0.61	0.61	3.8
210	W72M8	1280	1729	120	800	120	0.91	0.91	0.91
211	W72M6	1280	1729	120	800	120	1.19	1.19	1.19
212	W96M6	1280	1729	120	800	120	0.91	0.91	0.91
213	W96M8	1280	1729	120	800	120	1.19	1.19	1.19
214	W48M6	1280	1720	120	800	120	0.79	0.79	0.89
215	W72M8	1280	1720	120	800	120	0.91	0.91	0.89
216	W72M6	1280	1720	120	800	120	1.19	1.19	1.19
217	W72M8	1280	1720	120	800	120	0.91	0.91	0.89
218	W96M8	1280	1720	120	800	120	1.19	1.19	1.19
219	DP1	2340	2885	75	3045	95	0.76	0.82	0.62

220	DP2	2340	2885	75	3045	95	0.76	0.82	0.62
221	1F	2760	2000	80	200	200	0.4	0.4	3.98
222	2F	3520	2000	80	200	200	0.4	0.4	3.98
223	T03	1200	800	50	150	150	0.41	0.57	2.01
224	T06	1200	800	50	150	150	0.41	0.57	2.01
225	T07	1200	800	50	150	150	0.41	0.57	1.13
226	T08	1200	800	50	150	150	0.41	0.57	2.01
227	T09	1200	800	50	150	150	0.41	0.57	1.13
228	W-15-1	1000	2150	150	500	150	1.06	1.06	3.8
229	W-12-1	1000	2120	120	500	120	1.32	1.32	4.75
230	W-12-2	1000	2120	120	500	120	0.91	0.91	4.75
231	W-12-3	1000	2120	120	500	120	1.7	1.7	4.75
232	W-12-4	1000	2120	120	500	120	1.32	1.32	4.75
233	W-12-5	1000	2120	120	500	120	1.32	1.32	4.75
234	W-15-2	2000	2150	150	500	150	1.06	1.06	3.8
235	W-12-6	2000	2120	120	500	120	1.32	1.32	4.75
236	W-12-7	2000	2120	120	500	120	1.32	1.32	5.48
237	24M:8:30	1600	2150	150	1000	150	0.8	0.8	0.57
238	24M:8:40	1600	2150	150	1000	150	0.6	0.6	0.48
239	24M:8:50	1600	2150	150	1000	150	0.48	0.48	0.76
240	24M:6:30	1200	2150	150	1000	150	0.8	0.8	0.57
241	24M:6:40	1200	2150	150	1000	150	0.6	0.6	0.57
242	36M:12:30	2400	2150	150	1000	150	1.16	1.16	4.47
243	36M:12:40	2400	2150	150	1000	150	0.9	0.9	4.5
244	36M:12:50	2400	2150	150	1000	150	0.72	0.72	3.6
245	36L:8:30	1600	2150	150	1000	150	1.16	1.16	0.86
246	36L:8:40	1600	2150	150	1000	150	0.9	0.9	1.14
247	36M:8:30	1600	2150	150	1000	150	1.16	1.16	0.86
248	36M:8:40	1600	2150	150	1000	150	0.9	0.9	0.67
249	36M:8:50	1600	2150	150	1000	150	0.72	0.72	1.14
250	36M:6:30	1200	2150	150	1000	150	1.16	1.16	0.86
251	36M:6:40	1200	2150	150	1000	150	0.9	0.9	1.62
252	48M:8:30	1600	2150	150	1000	150	1.61	1.61	1.14
253	48M:8:40	1600	2150	150	1000	150	1.16	1.16	0.95
254	48M:8:50	1600	2150	150	1000	150	0.96	0.96	1.62
255	48H:8:30	1600	2150	150	1000	150	1.61	1.61	1.14
256	48H:8:40	1600	2150	150	1000	150	1.16	1.16	0.95
257	48H:8:50	1600	2150	150	1000	150	0.96	0.96	0.92
258	WC150	2250	1500	130	250	250	0.81	0.81	2.57
259	WD170	2250	1500	130	250	250	1.01	1.01	2.57
260	WD200	2250	1500	130	250	250	0.85	0.85	2.57
261	WCD170	2250	1500	130	250	250	1.01	1.01	2.57
262	WB-1	700	1120	50	150	120	0.25	0.25	4.23
263	WB-2	700	1120	50	150	120	0.25	0.25	4.23
264	WB-3	700	1120	50	150	120	0.25	0.25	4.23
265	WB-4	700	1120	50	150	120	0.25	0.25	4.23
266	WB-5	700	1120	50	150	120	0.25	0.25	4.23
267	WB-6	700	1120	50	150	120	0.5	0.5	4.23
268	WB-7	700	1120	50	150	120	0.5	0.5	4.23
269	WB-8	700	1120	50	150	120	0.5	0.5	4.23
270	WB-9	700	1120	50	150	120	0.25	0.25	4.23
271	WB-10	700	1120	50	150	120	0.25	0.25	4.23
272	WB-11	700	1120	50	150	120	0.25	0.25	4.23
273	WB-12	700	1120	50	150	120	0.25	0.25	4.23
274	WB-13	700	1120	50	150	120	0.25	0.25	4.23
275	WB-14	700	1120	50	150	120	0.25	0.25	4.23

276	WB-17	700	1120	50	150	120	0.25	0.25	4.23
277	HSCW1	1200	880	75	375	90	0.47	1.26	4
278	HSCW2	1200	880	75	375	90	0.47	1.26	4
279	HSCW3	1200	880	75	375	90	0.47	0.75	4
280	HSCW4	1200	880	75	375	90	0.47	0.75	4
281	HSCW5	1200	880	75	375	90	0.75	1.26	4
282	HSCW6	1200	880	75	375	90	0.75	1.26	4
283	HSCW7	1200	880	75	375	90	0.75	0.75	4
284	FSW-4	914.4	1219.2	76	152	152	0.55	0.55	3.27
285	FSW-5	914.4	1219.2	76	152	152	0.55	0.55	3.27
286	FSW-6	914.4	1219.2	76	152	152	0.55	0.55	3.27
287	FSW-7	914.4	1219.2	76	152	152	1.09	1.09	3.27
288	FSW-8	914.4	1219.2	76	152	152	0.23	0.23	3.27
289	FSW-9	914.4	1219.2	76	152	152	1.09	1.09	3.27
290	FSW-10	914.4	1219.2	76	152	152	1.09	1.09	3.27
291	FSW-12	914.4	1219.2	76	152	152	0.23	0.23	3.27
292	FSW-13	914.4	1219.2	76	152	152	0.23	0.23	3.27
293	1	600	1330	40	130	130	0.31	0.31	1.26
294	2	600	1330	40	130	130	0.63	0.63	1.26
295	3	600	1330	40	130	130	1.26	1.26	1.26
296	4	600	1330	30	130	130	0.84	0.84	1.26
297	5	600	1330	20	130	130	0.63	0.63	1.26
298	6	600	1330	20	130	130	1.26	1.26	1.26

Table A-1. (Continued)

No.	Specimen ID	f_c	f_{yh}	f_{yv}	f_{yb}	P/f_cA_w	V_{test}	V_n	V_n/V_{test}
1	WAS	27	377	377	434	0.07	654	603.6	0.92
2	WBS	27	377	377	434	0.07	542	546.2	1.01
3	5	22	271	271	324	0	378	336.7	0.89
4	6	22	271	271	324	0	360	336.7	0.94
5	7	26	271	271	305	0	511	375.3	0.73
6	8	25	271	271	305	0	483	365.9	0.76
7	9	24	271	271	305	0	535	356.3	0.67
8	10	23	271	271	305	0	454	346.5	0.76
9	12	31	271	271	324	0	523	421.2	0.81
10	13	18	393	393	296	0	414	344.1	0.83
11	14	21	414	414	299	0	489	378.9	0.77
12	25	41	331	331	276	0	409	543.3	1.33
13	32	27	345	345	345	0	445	423.9	0.95
14	33	24	341	341	341	0	476	394.7	0.83
15	35	26	345	345	345	0	405	414.5	1.02
16	36	25	341	341	341	0	454	404.3	0.89
17	37	28	345	345	345	0	360	433.2	1.20
18	40	34	323	323	345	0	676	482.7	0.71
19	41	23	323	323	345	0	471	381.6	0.81
20	43	34	323	323	345	0	560	482.7	0.86
21	44	32	323	323	345	0	592	465.2	0.79
22	45	20	313	313	345	0	409	477.7	1.17
23	46	12	296	296	345	0	387	344.8	0.89
24	47	18	294	294	345	0	489	444.2	0.91
25	48	19	336	336	345	0	489	465.6	0.95
26	49	14	319	319	319	0	400	382.6	0.96
27	50	16	306	306	319	0	409	456.6	1.12
28	51	17	343	343	319	0	503	483.0	0.96
29	52	18	348	348	316	0	498	500.2	1.00

30	53	21	341	341	317	0	520	544.2	1.05
31	54	14	346	346	312	0	427	434.6	1.02
32	56	23	371	371	316	0	792	833.8	1.05
33	57	21	349	349	316	0	783	782.8	1.00
34	59	19	348	348	314	0	676	741.1	1.10
35	B3-2	27	513	545	414	0	1108	980.0	0.88
36	B4-3	19	0	535	527	0	1017	738.5	0.73
37	B6-4	21	496	496	529	0	876	779.1	0.89
38	B8-5	23	496	527	489	0	851	745.7	0.88
39	4BII-1	20	359	359	312	0	89	95.5	1.07
40	3A2-3	22	359	359	312	0	155	175.4	1.13
41	4BII-3	20	359	359	312	0	201	242.4	1.21
42	BB	50.5	441	441	446	0	1940	2408.4	1.24
43	CW-0.6-1.2-20	34	412	412	379	0.06	1658	1335.5	0.81
44	CW-0.6-0.6-20	30	412	412	374	0.07	1179	1107.7	0.94
45	CW-0.6-0.8-20	40	412	412	379	0.05	1475	1310.5	0.89
46	CW-0.6-1.6-20	34	412	412	379	0.06	1677	1448.9	0.86
47	CW-0.6-2.0-20	35	412	412	379	0.06	1823	1582.6	0.87
48	CW-0.6-1.2-40	32	412	412	379	0.12	1515	1455.8	0.96
49	CW-0.4-1.2-20	33	412	412	379	0.06	1617	1447.0	0.89
50	CW-0.8-1.2-20	33	412	412	379	0.06	1343	1225.8	0.91
51	CW-0.6-0.6-20a	29	412	412	379	0.07	1246	1085.7	0.87
52	CW-0.6-0.8-20a	30	412	412	379	0.07	1307	1164.3	0.89
53	W7101	26	447	447	297	0.05	625	891.2	1.43
54	W7102	25	447	447	297	0.06	522	743.7	1.42
55	W7402	23	414	414	318	0.06	529	700.3	1.32
56	W7404	24	414	414	409	0.06	541	719.3	1.33
57	W7501	27	367	367	409	0.05	635	747.2	1.18
58	W7503	22	367	367	409	0.06	639	673.0	1.05
59	W7601	20	443	443	328	0.07	797	809.6	1.02
60	W7602	20	443	443	328	0.06	826	804.1	0.97
61	W7603	24	443	443	328	0.05	1008	1066.1	1.06
62	W7604	35	423	423	383	0.04	493	711.4	1.44
63	W7605	27	423	423	383	0.05	622	774.5	1.25
64	W7606	26	423	423	425	0.05	884	919.8	1.04
65	J1	103	610	610	630	0.05	1209	865.6	0.72
66	J4	94	610	610	630	0.05	810	715.3	0.88
67	J5	103	610	610	630	0.05	595	616.4	1.04
68	J6	97	610	578	630	0.05	724	609.9	0.84
69	J7	111	578	610	630	0.05	894	816.3	0.91
70	CW-0.6-0-20	35	0	0	374	0.06	1193	1015.7	0.85
71	CW-0.6-0.3-20	35	412	412	379	0.06	1283	1100.8	0.86
72	CW-0.6-2.4-20	34	412	412	379	0.06	2003	1664.3	0.83
73	CW-0.6-2.8-20	32	412	412	379	0.06	1732	1736.3	1.00
74	CW-0.6-0-0	32	0	0	379	0	744	792.3	1.06
75	CW-0.6-0-40	32	0	0	379	0.12	1421	1115.6	0.79
76	CW-0.6-0.6-0	35	412	412	379	0	1151	1013.7	0.88
77	CW-0.6-0.6-40	34	412	412	374	0.12	1698	1334.0	0.79
78	CW-0.4-0.6-20	34	412	412	374	0.06	1871	1273.5	0.68
79	CW-0.8-0.6-20	34	412	412	374	0.06	1275	1075.5	0.84
80	CW-0.4-2.0-20	34	412	412	374	0.06	2081	1730.3	0.83
81	CW-0.8-2.0-20	34	412	412	379	0.06	1656	1470.0	0.89
82	CW-0.6-2-0	34	412	412	379	0	1712	1393.6	0.81
83	CW-0.6-2-40	34	412	412	379	0.12	2035	1730.9	0.85
84	CW-0.6-2-20B	36	412	412	374	0.06	1775	1602.9	0.90
85	CW-0.6-0.6-20L	25	412	412	387	0.08	1276	1018.0	0.80

86	CW-0.6-1.2-20L	26	412	412	387	0.08	1390	1211.7	0.87
87	CW-0.6-2-20L	25	412	412	387	0.08	1491	1414.8	0.95
88	Kabeyasawa-K7	20	356	356	378	0.07	738	999.2	1.35
89	Taga-No 1	27	412	412	387	0.07	1088	1165.6	1.07
90	Taga-No 2	38	412	412	387	0.05	1334	1331.1	1.00
91	Taga-No 3	58	412	412	387	0.03	1461	1595.1	1.09
92	Taga-No 4	37	412	412	387	0.05	1236	1142.7	0.92
93	Taga-No 5	26	412	412	387	0.08	1137	1393.0	1.23
94	Taga-No 6	37	412	412	387	0.05	1461	1539.6	1.05
95	Taga-No 7	58	412	412	387	0.03	1677	1821.8	1.09
96	S-1	79	578	545	532	0	428	555.0	1.30
97	S-2	65	578	545	533	0.07	720	590.9	0.82
98	S-3	69	578	545	532	0.13	851	694.9	0.82
99	S-4	75	578	533	532	0	600	559.9	0.93
100	S-5	73	578	533	531	0.06	790	638.4	0.81
101	S-6	71	578	533	532	0.12	970	713.6	0.74
102	S-7	71	545	545	533	0.06	800	676.2	0.85
103	S-F	61	578	545	561	0.04	487	531.6	1.09
104	Aoyagi_1-1-148	20	353	353	363	0	931	876.3	0.94
105	Aoyagi_1-2-149	26	353	353	363	0	1029	1010.3	0.98
106	Aoyagi_1-3-150	29	339	339	363	0	1553	2055.9	1.32
107	Aoyagi_1-4-151	24	353	353	272	0	1495	966.8	0.65
108	Aoyagi_1-5-152	29	339	339	272	0	2308	2055.9	0.89
109	Endo-1	26	624	624	359	0.05	654	895.5	1.37
110	Endo-2	25	624	624	359	0.06	522	753.3	1.44
111	Endo-3	26	624	624	359	0.05	524	752.5	1.44
112	Endo-4	25	624	624	359	0.07	467	506.8	1.09
113	Endo-5	26	624	624	359	0.07	783	817.2	1.04
114	Ryo_1-1-29	23	335	467	467	0	965	668.6	0.69
115	Ryo_1-2-30	33	335	467	467	0	931	816.2	0.88
116	Ryo_2-1-32	17	485	467	467	0	343	334.1	0.97
117	Ryo_2-3-34	17	485	467	467	0	470	334.1	0.71
118	70	24	549	549	419	0	834	651.2	0.78
119	Sugano-71	25	461	461	419	0	804	701.3	0.87
120	Sugano-140	21	572	572	397	0.09	2353	2880.0	1.22
121	Sugano-141	21	572	572	397	0.17	2942	3320.8	1.13
122	Sugano-142	21	572	572	397	0.11	3138	2990.2	0.95
123	Sugano-143	20	572	572	397	0.07	1814	2320.6	1.28
124	Sugano-144	21	572	572	397	0.07	1912	2387.9	1.25
125	Sugano-145	20	284	284	397	0.08	2138	2383.4	1.11
126	Sugano-146	20	284	284	397	0.08	1981	2383.4	1.20
127	Sugano-147	21	397	397	397	0.09	2305	2727.8	1.18
128	Tsuboi-131	31	296	296	302	0	162	177.2	1.09
129	Tsuboi-133	32	296	296	302	0	174	218.3	1.25
130	Tsuboi-134	30	296	296	261	0	195	180.2	0.92
131	Tsuboi-135	29	296	296	302	0	184	177.6	0.97
132	W1	37	450	450	465	0	491	589.2	1.20
133	W2	36	450	450	465	0	621	666.0	1.07
134	W3	38	450	450	465	0	569	678.1	1.19
135	W4	36	450	450	465	0	622	791.2	1.27
136	Ohono_2-1	29	280	224	224	0	294	279.7	0.95
137	Ohono_2-2	29	280	224	224	0	282	279.7	0.99
138	Ohono_2-3	29	280	224	224	0	231	168.7	0.73
139	Ohono_2-4	29	280	224	224	0	210	168.7	0.80
140	Ohono_2-5	29	224	280	224	0	210	180.0	0.86
141	Ohono_2-6	29	224	280	224	0	207	180.0	0.87

142	NW-2	56	1001	848	776	0.1	714	950.2	1.33
143	No.1	65	792	792	1009	0.13	1101	999.0	0.91
144	No.2	71	792	792	1009	0.12	1208	1112.2	0.92
145	No.3	72	792	792	1009	0.12	1360	1215.7	0.89
146	No.4	103	792	792	1009	0.14	1656	1541.1	0.93
147	No.6	74	1420	1420	1009	0.12	1353	1576.5	1.17
148	No.7	72	792	792	1009	0.12	1478	1462.2	0.99
149	No.8	76	792	792	1009	0.11	1638	1710.8	1.04
150	DHSCW-01	77	474	424	460	0.28	739	997.9	1.35
151	DHSCW-02	77	474	424	460	0.21	649	912.1	1.41
152	DHSCW-03	77	474	424	460	0.21	915	1052.4	1.15
153	DHSCW-04	77	474	424	460	0.21	902	1052.4	1.17
154	DHSCW-05	77	474	424	460	0.21	1179	1291.7	1.10
155	DHSCW-06	77	474	424	460	0.21	1072	1291.7	1.20
156	HP0D0	36	335	554	554	0	890	838.4	0.94
157	HP5D0	36	335	554	554	0.01	975	859.5	0.88
158	S1	37	574	574	574	0.07	680	847.6	1.25
159	S2	38	574	574	574	0.26	928	1153.8	1.24
160	S3	37	574	574	530	0.07	977	963.3	0.99
161	S5	37	574	574	574	0.06	682	832.7	1.22
162	S6	36	537	479	479	0.07	667	723.2	1.08
163	S7	34	555	555	555	0.27	855	1088.2	1.27
164	W1	34	327	327	460	0	397	308.9	0.78
165	W2	31	429	429	460	0	400	299.3	0.75
166	W3	31	429	429	460	0	379	299.3	0.79
167	W4	37	359	359	460	0	414	328.6	0.79
168	W5	32	359	359	460	0	346	276.2	0.80
169	S4	46	667	653	617	0.07	2544	1893.2	0.74
170	S4	47	667	653	617	0.07	2545	1915.0	0.75
171	HN4-1	32	302	302	302	0	205	281.1	1.37
172	HN4-2	32	302	302	302	0	247	281.1	1.14
173	HN4-3	32	302	302	302	0	202	281.1	1.39
174	HN6-1	30	443	443	443	0	255	293.6	1.15
175	HN6-2	30	443	443	443	0	204	293.6	1.44
176	HM4-1	38	302	302	302	0	223	310.8	1.39
177	HM4-2	38	302	302	302	0	231	310.8	1.35
178	HM4-3	40	302	302	302	0	250	320.3	1.28
179	LN4-1	18	302	302	302	0	193	204.1	1.06
180	LN4-2	18	302	302	302	0	217	204.1	0.94
181	LN4-3	30	302	302	302	0	203	270.8	1.33
182	LN6-1	31	443	443	443	0	246	298.8	1.21
183	H-HZ4	15	259	259	226	0	30	27.2	0.91
184	H-HZ6	16	259	259	226	0	30	28.3	0.94
185	H-HZ8	16	259	259	226	0	33	28.3	0.86
186	H-HZ10	18	259	259	226	0	28	30.3	1.08
187	L-C	21	508	508	475	0.1	1052	909.1	0.86
188	L-M	21	508	508	475	0.1	995	909.1	0.91
189	M-C	40	508	508	475	0.07	1142	1243.4	1.09
190	M-V	40	508	508	475	0.07	1201	1410.4	1.17
191	M-H	40	508	508	475	0.07	1131	1243.4	1.10
192	U-1	29	391	391	391	0.04	1636	1475.4	0.90
193	U-2	29	391	391	391	0.04	1618	1475.5	0.91
194	RA-00P	32	349	349	349	0	1473	1398.3	0.95
195	RA-15P	30	349	349	381	0.03	1671	1451.3	0.87
196	RB-00P	29	381	381	381	0	1264	1283.9	1.02
197	RB-15P	29	381	381	349	0.04	1464	1398.7	0.96

198	RC-00P	30	349	349	349	0	1032	1206.8	1.17
199	RC-15P	29	349	349	349	0.04	1170	1292.4	1.10
200	SW1	86	536	536	535	0.1	1000	719.0	0.72
201	SW2	86	498	498	535	0.1	1191	858.9	0.72
202	SW3	96	536	498	535	0.09	1099	806.2	0.73
203	SW4	96	536	498	535	0	718	648.8	0.90
204	SW5	83	536	498	535	0.11	1104	753.6	0.68
205	SW6	83	498	498	419	0.11	1121	796.1	0.71
206	Type N	22	340	340	398	0.11	712	632.3	0.89
207	Type S	25	340	340	398	0.1	702	670.5	0.96
208	Matui_1-3	12	237	237	237	0	76	67.6	0.89
209	Matui_1-4	12	237	237	237	0	72	72.5	1.01
210	W72M8	82	792	792	792	0.02	2066	2277.2	1.10
211	W72M6	82	560	560	560	0.02	2015	2232.4	1.11
212	W96M6	102	792	792	792	0.02	2128	2554.9	1.20
213	W96M8	102	792	792	792	0.02	2483	2737.8	1.10
214	W48M6	82	560	560	560	0.02	1516	2033.4	1.34
215	W72M8	82	792	792	792	0.02	2066	2261.8	1.09
216	W72M6	82	560	560	560	0.02	2015	2217.2	1.10
217	W72M8	102	792	792	792	0.02	2128	2537.5	1.19
218	W96M8	102	792	792	792	0.02	2483	2719.6	1.10
219	DP1	22	605	605	605	0.05	1277	1177.1	0.92
220	DP2	19	605	605	605	0	891	1005.7	1.13
221	1F	28	377	377	434	0.06	686	602.4	0.88
222	2F	27	377	377	434	0.07	554	546.2	0.99
223	T03	30	420	420	420	0	129	128.8	1.00
224	T06	34	420	420	420	0	117	137.1	1.17
225	T07	31	420	420	420	0.1	137	162.7	1.19
226	T08	31	420	420	420	0.07	144	153.2	1.06
227	T09	27	420	420	420	0	94	122.3	1.30
228	W-15-1	25	369	369	369	0.08	2187	2078.2	0.95
229	W-12-1	35	369	369	369	0.06	2658	1990.9	0.75
230	W-12-2	38	369	369	369	0.05	2511	1870.5	0.74
231	W-12-3	36	369	369	369	0.06	2511	2171.5	0.86
232	W-12-4	36	369	369	369	0.03	2481	1893.5	0.76
233	W-12-5	40	369	369	369	0.05	2668	2089.0	0.78
234	W-15-2	26	369	369	369	0.08	1814	1787.7	0.99
235	W-12-6	33	369	369	369	0.06	1755	1637.4	0.93
236	W-12-7	34	369	369	422	0.03	1648	1564.7	0.95
237	24M:8:30	38	296	296	422	0.05	1680	1972.5	1.17
238	24M:8:40	36	422	422	528	0.06	1740	1978.2	1.14
239	24M:8:50	35	528	528	296	0.06	1740	1946.2	1.12
240	24M:6:30	40	296	296	422	0.05	2100	2205.0	1.05
241	24M:6:40	41	422	422	296	0.05	2190	2259.3	1.03
242	36M:12:30	36	296	296	422	0.06	2490	1855.2	0.75
243	36M:12:40	34	422	422	528	0.06	2490	1855.0	0.74
244	36M:12:50	37	528	528	528	0.05	2430	1896.0	0.78
245	36L:8:30	25	296	296	422	0.08	1800	1793.7	1.00
246	36L:8:40	28	422	422	296	0.07	1830	1913.0	1.05
247	36M:8:30	39	296	296	422	0.05	1890	2139.8	1.13
248	36M:8:40	39	422	422	528	0.05	2040	2186.5	1.07
249	36M:8:50	38	528	528	296	0.05	1980	2156.3	1.09
250	36M:6:30	33	296	296	422	0.06	2250	2151.4	0.96
251	36M:6:40	35	422	422	296	0.06	2370	2270.2	0.96
252	48M:8:30	27	296	296	422	0.07	1980	2001.3	1.01
253	48M:8:40	28	422	422	528	0.07	2040	2053.7	1.01

254	48M:8:50	28	528	528	296	0.07	2040	2076.0	1.02
255	48H:8:30	42	296	296	422	0.05	2280	2401.1	1.05
256	48H:8:40	43	422	422	528	0.05	2340	2447.4	1.05
257	48H:8:50	45	528	528	349	0.05	2430	2528.5	1.04
258	WC150	27.3	451.3	451.3	547.9	0.07	870	897.1	1.03
259	WD170	32.9	505.9	595.7	595.7	0.07	980	1130.1	1.15
260	WD200	33.7	451.3	574.9	547.9	0.07	880	1013.3	1.15
261	WCD170	33.9	505.9	595.7	595.7	0.07	890	1142.9	1.28
262	WB-1	18	294	382	383	0	173	172.0	0.99
263	WB-2	18	294	382	383	0	184	172.0	0.93
264	WB-3	16	294	382	383	0	210	159.8	0.76
265	WB-4	16	294	382	383	0	226	159.8	0.71
266	WB-5	15	294	382	383	0.17	334	231.9	0.69
267	WB-6	15	294	382	383	0	235	171.5	0.73
268	WB-7	15	294	382	383	0.16	304	245.2	0.81
269	WB-8	15	294	382	383	0.32	282	318.9	1.13
270	WB-9	17	530	530	383	0.15	240	251.5	1.05
271	WB-10	17	530	530	383	0.15	238	251.5	1.06
272	WB-11	17	530	530	383	0.15	277	251.5	0.91
273	WB-12	17	530	530	383	0.15	332	251.5	0.76
274	WB-13	17	530	530	383	0.15	216	251.5	1.16
275	WB-14	17	530	530	383	0.15	203	251.5	1.24
276	WB-17	10	530	530	383	0.25	193	216.9	1.12
277	HSCW1	104	550	550	550	0.04	735	582.8	0.79
278	HSCW2	93	550	550	550	0.09	845	612.6	0.72
279	HSCW3	86	550	550	550	0.09	625	569.4	0.91
280	HSCW4	91	550	550	550	0.22	866	756.0	0.87
281	HSCW5	84	550	550	550	0.09	801	619.7	0.77
282	HSCW6	90	550	550	550	0.05	745	591.7	0.79
283	HSCW7	102	550	550	550	0.08	800	657.4	0.82
284	FSW-4	50	419	419	425	0.09	606	711.5	1.17
285	FSW-5	56	419	419	425	0.04	633	674.7	1.07
286	FSW-6	50	419	419	425	0.02	453	596.5	1.32
287	FSW-7	53	419	419	425	0.04	702	731.5	1.04
288	FSW-8	48	600	600	425	0.05	553	597.5	1.08
289	FSW-9	50	419	419	425	0.05	737	725.1	0.98
290	FSW-10	56	419	419	425	0.08	824	825.1	1.00
291	FSW-12	57	600	600	425	0.08	676	721.7	1.07
292	FSW-13	57	600	600	425	0.01	474	595.7	1.26
293	1	36	286	286	286	0.19	373	446.3	1.20
294	2	30	286	286	286	0.2	370	422.6	1.14
295	3	32	286	286	286	0.22	438	495.5	1.13
296	4	33	286	286	286	0.22	276	359.0	1.30
297	5	30	286	286	286	0.31	211	254.0	1.20
298	6	34	286	286	286	0.29	213	286.5	1.35
								AVG	1.00
								COV	0.19

Table A- 2. Test result of RWs

No.	Specimen ID	h_w	l_w	t_w	b_b	h_b	ρ_h	ρ_v	ρ_b
1	C10	3750	2250	200	200	410	0.6	0.56	2.45
2	A10	3750	2250	200	200	410	0.6	0.56	2.45
3	A14	3750	2250	200	200	410	0.6	0.56	2.45
4	A20	3750	2250	200	200	410	0.6	0.56	2.45
5	W-MC-C	3316.7	1525	203	203	153	0.55	0.42	6.58

6	W-MC-N	3316.7	1525	203	203	153	0.55	0.42	6.58
7	RC-M-1.2	1200	1000	100	100	150	0.63	0.63	3.54
8	RC-H-1.2	1200	1000	100	100	150	0.86	0.86	6.46
9	RC-M-1.5	1500	1000	100	100	150	0.63	0.63	6.46
10	RC-H-1.5	1500	1000	100	100	150	0.69	0.69	8.85
11	H0.33OR	750	1500	200	200	150	1.59	1.06	1.06
12	H0.33OUC	750	1500	200	200	150	1.59	1.06	1.06
13	H0.33ORC	750	1500	200	200	150	1.59	1.06	1.06
14	H0.33OGC	750	1500	200	200	150	1.59	1.06	1.06
15	H0.33OR-HC-LD	750	1500	200	200	150	1.59	2.06	2.06
16	H0.33OU-HC-F	750	1500	200	600	200	1.59	1.51	1.51
17	H0.33OU	750	1500	200	200	150	1.59	1.06	1.06
18	N0.33MR	750	1500	200	200	150	1.59	1.06	1.06
19	H0.33MR	750	1500	200	200	150	1.59	0.66	0.66
20	H0.33OU-HC-LD	750	1500	200	200	150	1.59	2.06	2.06
21	PW1	4691	3048	152	152	305	0.28	0.28	3.5
22	PW2	4691	3048	152	152	305	0.28	0.28	3.5
23	PW3	4691	3048	152	152	305	0.28	1.57	2
24	PW4	4691	3048	152	152	305	0.28	0.28	3.5
25	SW-13	1905	1905	76	76	191	0.93	2.87	2.87
26	MCN50M	2498.08	2402	102	102	240	0.14	0.14	3.27
27	MCN50C	2494.96	2399	102	102	240	0.14	0.14	3.27
28	MCN100C	2492.88	2397	101	101	240	0.28	0.28	4.69
29	MRN100C	2484	5400	100	100	200	0.28	0.28	2.84
30	MRN50mC	2482.16	5396	103	103	200	0.12	0.12	2.91
31	MCN50mC	2493.92	2398	103	103	240	0.12	0.12	3.45
32	MEN50mC	2502.78	1239	101	101	124	0.12	0.12	4.54
33	MCN50mD	2318.36	1916	83	83	192	0.11	0.11	3.77
34	MCN100D	2324.41	1921	84	84	192	0.26	0.26	4.96
35	S5-Z4B2-2	2250	2000	200	200	300	0.25	0.7	1.34
36	M60	2159	2032	203	203	254	0.34	0.34	4.04
37	M115	2159	2032	203	203	254	0.17	0.17	2.33
38	H60	2159	2032	203	203	254	0.86	0.86	6.63
39	H115	2159	2032	203	203	254	0.43	0.43	3.51
40	H60X	2159	2032	203	203	254	0.86	0.86	6.63
41	EB	2159	2032	203	203	406	0.82	0.82	4.6
42	3B	2159	2032	203	203	254	0.82	0.82	5.16
43	Sheu-SWN-1D	500.38	1000.76	100	100	100	0.57	0.43	0.43
44	Sheu-SW-0E	500.38	1000.76	100	100	100	0.71	0.71	0.71
45	Sheu-SW-1E	500.38	1000.76	100	100	100	0.71	0.71	0.71
46	Sheu-SW-9E	749.3	1000.76	100	100	100	1.18	1.27	1.27
47	Sheu-SW-1	500.38	1000.76	100	100	100	0.57	0.43	0.43
48	Sheu-SW-4	500.38	1000.76	100	100	100	1.03	0.77	0.77
49	Sheu-SW-4A	500.38	1000.76	100	100	100	1.03	0.77	0.77
50	Sheu-SW-6	500.38	1000.76	100	100	100	1.03	0.77	0.77
51	Sheu-SW9	500.38	1000.76	100	100	100	0.57	0.79	0.79
52	Sheu-SW10	500.38	1000.76	100	100	100	0.57	0.76	0.76
53	Sheu-SW11	500.38	1000.76	100	100	100	0.57	0.79	0.79
54	Sheu-SW12	500.38	1000.76	100	100	100	0.57	0.78	0.78
55	Sheu-SW13	500.38	1000.76	100	100	100	0	0.76	0.76
56	Sheu-SW14	500.38	1000.76	100	100	100	1.14	0.76	0.76
57	Sheu-SW15	749.3	1000.76	100	100	100	0.57	0.79	0.79
58	Sheu-SW16	749.3	1000.76	100	100	100	0.57	0.76	0.76
59	Sheu-SW18	749.3	1000.76	100	100	100	0.57	0.78	0.78
60	Sheu-SW19	749.3	1000.76	100	100	100	0	0.76	0.76
61	Sheu-SW20	749.3	1000.76	100	100	100	0.57	0.76	0.76

62	W2	2000	1500	200	200	200	0.29	0.32	1.28
63	10	1801	1300	80	80	130	0.25	0.25	7.31
64	11	1400	1400	100	100	140	0.13	0.26	5.71
65	13	1400	1400	100	100	140	0.26	0.26	5.71
66	14	1199	1700	80	80	170	0.13	0.25	4.41
67	28	1400	1400	100	100	140	0	0.25	4.29
68	73	1700	1700	160	160	170	0.26	0.51	5.68
69	74	1700	1700	160	160	170	0.57	0.51	5.68
70	75	1700	1700	160	160	170	0.57	0.51	5.68
71	76	1700	1700	160	160	170	1.08	0.51	5.68
72	77	1700	1700	160	160	170	1.08	0.51	5.68
73	78	1700	1700	160	160	170	0.61	0.51	2.51
74	79	1700	1700	160	160	170	0.61	0.51	2.51
75	80	1700	1700	160	160	170	1.08	0.51	2.51
76	81	1700	1700	160	160	170	1.08	0.51	2.51
77	82	1700	850	160	160	85	0.57	0.4	9.91
78	83	1700	850	160	160	85	0.57	0.4	9.91
79	Yoshizaki-165	860	800	60	60	86	0.23	0.22	4.92
80	Yoshizaki-166	860	800	60	60	86	0.82	0.73	5.47
81	Yoshizaki-167	860	800	60	60	86	0.41	0.44	7.71
82	Yoshizaki-168	860	800	60	60	86	0.82	0.73	8.25
83	Yoshizaki-169	860	800	60	60	86	1.17	1.17	8.25
84	Yoshizaki-170	860	1200	60	60	120	0.23	0.24	3.52
85	Yoshizaki-171	860	1200	60	60	120	0.82	0.78	3.91
86	Yoshizaki-172	860	1200	60	60	120	0.41	0.44	5.52
87	Yoshizaki-173	860	1200	60	60	120	0.82	0.78	5.91
88	Yoshizaki-174	860	1200	60	60	120	1.17	1.17	5.91
89	Yoshizaki-176	860	1600	60	60	160	0.82	0.8	2.94
90	Yoshizaki-177	860	1600	60	60	160	0.41	0.37	4.44
91	Yoshizaki-178	860	1600	60	60	160	0.82	0.8	4.44
92	Yoshizaki-179	860	1600	60	60	160	1.17	1.17	4.73
93	WSL1	1750	1600	100	100	300	0.2	0.2	4.02
94	WSL2	1750	1600	100	100	300	0.2	0.2	1.34
95	WSL5	1750	1600	100	100	300	0.2	0.2	4.02
96	WSL7	1750	1600	80	80	300	0.68	0.25	3.35
97	WSL8	1750	1600	80	80	300	0.48	0.17	3.35
98	SW11	825	750	70	70	140	1.1	2.4	3.1
99	SW12	825	750	70	70	140	1.1	2.4	3.1
100	SW13	825	750	70	70	140	1.1	2.4	3.1
101	SW14	825	750	70	70	140	1.1	2.4	3.1
102	SW15	825	750	70	70	140	1.1	2.4	3.1
103	SW16	825	750	70	70	140	1.1	2.4	3.1
104	SW17	825	750	70	70	140	1.1	2.4	3.1
105	SW22	1375	650	65	65	140	0.8	2.5	3.3
106	SW23	1375	650	65	65	140	0.8	2.5	3.3
107	SW31	1375	650	65	65	140	0.35	1.5	3.3
108	SW32	1375	650	65	65	140	0.35	1.5	3.3
109	SW32R	1375	650	65	65	140	0.35	1.5	3.3
110	SW33	1375	650	65	65	140	0.35	1.5	3.3
111	SW33R	1375	650	65	65	140	0.35	1.5	3.3
112	C30-N-ALR01	1000	800	80	80	80	1.44	1.96	2.45
113	C30-N-ALR02	1000	800	80	80	80	1.44	1.96	2.45
114	SW11	1646	3048	203	203	406	0.67	0.67	1.5
115	SW12	1646	3048	203	203	406	0.33	0.33	2
116	SW2	1647	3050	203	203	305	0.96	0.96	0.96
117	SW3	1647	3050	203	203	305	0.71	0.71	0.71

118	SW5	1006.5	3050	203	203	305	0.96	0.96	0.96
119	SW6	1006.5	3050	203	203	305	0.71	0.71	0.71
120	SW7	1006.5	3050	203	203	305	0.34	0.34	0.34
121	SW8	1647	3050	203	203	305	1.5	1.5	1.5
122	SW9	1647	3050	203	203	305	0.71	1.5	1.5
123	SW10	1647	3050	203	203	305	0.34	1.5	1.5
124	test1	760	1520	152	152	152	0.28	0.43	3.48
125	test4	760	1520	152	152	152	0.28	0.43	3.48
126	test2	760	1520	152	152	152	0.28	0.4	1.44
127	test3	760	1520	152	152	152	0.28	0.4	1.15
128	test9	610	1370	152	152	137	0.28	0.23	1.27
129	test7	610	1370	152	152	137	0.28	0.23	1.27
130	test8	610	1370	152	152	137	0.28	0.23	1.27
131	test5	610	1370	152	152	137	0.28	0.23	1.27
132	test6	610	1370	152	152	137	0.28	0.23	1.27
133	SW4	1200	600	60	60	110	0.39	0.5	6.86
134	SW7	1200	600	60	60	60	0.39	0.59	12.75
135	SW8	1200	600	60	60	110	0.28	0.5	7.14
136	SW9	1200	600	60	60	110	0.56	0.5	7.14
137	Wall-1	1160	2000	100	100	320	0.26	0.8	1.25
138	Wall-2	660	2000	100	100	320	0.26	0.8	1.25
139	Wall-7	1637.5	2000	100	100	320	0.24	0.34	0.89
140	Wall-8	1637.5	1500	100	100	360	0.24	0.37	0.79
141	WR-20	2250	1500	200	200	200	0.28	0.32	1.33
142	WR-10	2250	1500	200	200	200	0.28	0.32	1.33
143	WR-0	2250	1500	200	200	200	0.28	0.32	1.33
144	W4	1160	2000	100	100	260	0.57	0.33	1.09
145	W5	1160	2000	100	100	260	0.81	0.65	1.09
146	B14CD8U	2500	1300	150	150	240	0.67	0.67	2.57
147	SW2	1647	3050	203	203	305	1	1	1
148	SW3	1647	3050	203	203	305	0.67	0.67	0.67
149	T01	1200	800	80	80	150	0.51	0.71	1.41
150	T04	1200	800	80	80	150	0	0.71	1.41
151	T05	1200	800	80	80	150	0.51	0.71	2.51
152	T11	1200	800	80	80	150	0.51	0.71	1.41
153	MSW5	1900	1200	100	100	120	0.28	0.28	1.3
154	LSW1	1300	1200	100	100	120	0.57	0.57	1.7
155	LSW2	1300	1200	100	100	120	0.28	0.28	1.3
156	LSW3	1300	1200	100	100	120	0.28	0.28	1.3
157	LSW4	1300	1200	100	100	120	0.28	0.28	1.3
158	LSW5	1300	1200	100	100	120	0.28	0.28	1.3
159	W9	1500	750	125	125	75	0.2	1.05	2.41
160	W11	1500	750	125	125	75	0.11	1.05	2.41
161	W13	1500	750	125	125	75	0.11	1.05	2.41
162	T2-S2-3	950	1500	120	120	290	0.68	0.68	2.31
163	T2-S3-4	950	1500	120	120	290	0.68	0.68	2.31
164	T4-S1-6	700	1500	120	120	290	0.68	0.68	1.77
165	T5-S1-7	1700	1500	120	120	290	0.68	0.34	4.37
166	T6-S1-8	1700	1500	120	120	290	0.68	0.68	4.37
167	T1-S2-9	950	1500	120	120	290	0.34	0.34	2.31
168	SW23C2	1650	970	50	50	100	0.26	0.26	2.15
169	SW60N1	1650	970	50	50	100	0.38	0.38	5.44
170	SW60N2	1650	970	50	50	100	0.38	0.38	5.44
171	SW60C1	1650	970	50	50	100	0.38	0.38	5.44
172	SW60C2	1650	970	50	50	100	0.38	0.38	5.44
173	RW-A20-P10-S38	2440	1220	152	152	206	0.27	0.27	3.24

174	RW-A20-P10-S63	2440	1220	152	152	206	0.62	0.62	7.28
175	RW-A15-P10-S51	1830	1220	152	152	206	0.33	0.33	3.24
176	RW-A15-P10-S78	1830	1220	152	152	206	0.74	0.74	6.17
177	RW-A15-P2.5-S64	1830	1220	152	152	206	0.62	0.62	6.17
178	Wall 1	1646	3048	203	203	305	0.71	0.71	0.71
179	Wall 2	1646	3048	203	203	305	0.71	0.71	0.71
180	SH–CFP–M	1350	1060	150	150	106	0.52	1.56	1.56
181	SH–DCM–M	1350	1060	150	150	106	0.52	1.56	3.05
182	SH–CFP–C	1350	1060	150	150	106	0.52	1.56	1.56
183	SH–DCM–C	1350	1060	150	150	106	0.52	1.56	1.56
184	H0.1S	2000	1000	100	100	220	0.33	0.33	5.43
185	U1.0-BC	1350	1200	100	100	240	0.84	0.48	1.31
186	U1.0-BC2	1350	1200	100	100	240	0.84	0.48	1.31
187	Ohono_1-2	400	900	100	100	90	0.1	0.1	5
188	M4	609.6	899.16	80	80	90	0.26	0.39	0.39
189	C1.0	1350	1200	100	100	210	0.84	0.32	2.24

Table A-2. (Continued)

No.	Specimen ID	f_c	f_{yh}	f_{yv}	f_{yb}	$N/(f_c A_w)$	V_{test}	V_n	V_n/V_{test}
1	C10	32.7	507	507	543	0.09	1232	1387.6	1.13
2	A10	32.7	507	507	543	0.09	1221	1387.6	1.14
3	A14	42.6	507	507	543	0.14	1445	1577.2	1.09
4	A20	43.7	507	507	543	0.2	1641	1690.9	1.03
5	W-MC-C	33	483	427	462	0.03	716	871.7	1.22
6	W-MC-N	34	483	427	462	0.03	698	876.9	1.26
7	RC-M-1.2	46	667	667	484	0	345	361.6	1.05
8	RC-H-1.2	46	633	633	472	0	465	425.3	0.91
9	RC-M-1.5	47	667	667	472	0	350	373.1	1.07
10	RC-H-1.5	42	622	622	478	0	530	368.9	0.70
11	H0.33OR	31	655	655	655	0	1508	1609.7	1.07
12	H0.33OUC	27	655	655	655	0	1372	1562.9	1.14
13	H0.33ORC	27	655	655	655	0	1485	1562.9	1.05
14	H0.33OGC	27	655	655	655	0	1359	1562.9	1.15
15	H0.33OR-HC-LD	50	655	670	670	0	2638	2390.8	0.91
16	H0.33OU-HC-F	50	655	655	655	0	2465	2060.4	0.84
17	H0.33OU	31	655	655	655	0	1256	1609.7	1.28
18	N0.33MR	31	466	466	466	0	1073	1291.7	1.20
19	H0.33MR	31	655	655	655	0	1069	1388.3	1.30
20	H0.33OU-HC-LD	50	655	670	670	0	2178	2390.8	1.10
21	PW1	36	522	579	579	0.1	836	1047.0	1.25
22	PW2	40	522	579	579	0.13	1228	1147.5	0.93
23	PW3	34	522	353	353	0.1	1005	1188.3	1.18
24	PW4	29	522	462	462	0.12	970	971.7	1.00
25	SW-13	43	455	448	448	0	632	691.2	1.09
26	MCN50M	19	447	447	434	0.01	408	292.2	0.72
27	MCN50C	18	447	447	434	0.01	352	283.7	0.81
28	MCN100C	18	447	447	430	0.01	453	353.2	0.78
29	MRN100C	16	447	447	443	0.02	766	937.3	1.22
30	MRN50mC	20	605	605	456	0.01	776	916.2	1.18
31	MCN50mC	20	605	605	443	0.01	329	314.4	0.96
32	MEN50mC	20	605	605	443	0.01	154	136.8	0.89
33	MCN50mD	25	630	630	411	0.01	234	212.5	0.91
34	MCN100D	25	435	435	411	0.01	274	252.0	0.92
35	S5-Z4B2-2	39	327	465	488	0.4	1166	1566.2	1.34
36	M60	39	453	453	440	0	1122	888.3	0.79

37	M115	38	786	786	770	0	1104	837.2	0.76
38	H60	44	475	475	450	0	1969	1446.7	0.73
39	H115	44	806	806	770	0	1808	1323.3	0.73
40	H60X	42	475	475	450	0	1954	1426.4	0.73
41	EB	44.7	441	441	446	0	1680	1360.3	0.81
42	3B	49.1	441	441	446	0	1950	1403.8	0.72
43	Sheu-SWN-1D	27	467	467	467	0.12	299	317.0	1.06
44	Sheu-SW-0E	25	491	491	491	0	315	301.5	0.96
45	Sheu-SW-1E	34	491	491	491	0	324	336.4	1.04
46	Sheu-SW-9E	29	453	453	453	0	336	379.6	1.13
47	Sheu-SW-1	26	483	483	483	0	210	253.7	1.21
48	Sheu-SW-4	26	481	481	481	0	279	335.9	1.20
49	Sheu-SW-4A	27	481	481	481	0	272	339.9	1.25
50	Sheu-SW-6	28	481	481	481	0	276	343.9	1.25
51	Sheu-SW9	26	467	432	432	0	248	289.8	1.17
52	Sheu-SW10	27	467	453	453	0	270	294.7	1.09
53	Sheu-SW11	26	467	432	432	0	222	289.8	1.31
54	Sheu-SW12	26	467	448	448	0	248	292.1	1.18
55	Sheu-SW13	32	0	453	453	0	243	270.2	1.11
56	Sheu-SW14	31	467	453	453	0	313	354.3	1.13
57	Sheu-SW15	26	467	432	432	0	222	258.9	1.17
58	Sheu-SW16	26	467	453	453	0	221	259.5	1.17
59	Sheu-SW18	26	467	448	448	0	219	260.5	1.19
60	Sheu-SW19	25	0	453	453	0	157	190.2	1.21
61	Sheu-SW20	21	467	453	453	0	211	241.6	1.15
62	W2	28	335	335	395	0.1	443	546.5	1.23
63	10	16	367	367	471	0	187	118.6	0.63
64	11	16	362	362	471	0	235	150.1	0.64
65	13	18	370	370	471	0	289	182.7	0.63
66	14	17	366	366	471	0	255	173.6	0.68
67	28	23	0	431	471	0	258	162.8	0.63
68	73	21	419	407	376	0.09	775	514.4	0.66
69	74	21	421	407	376	0.09	790	632.0	0.80
70	75	14	421	407	376	0.14	812	581.7	0.72
71	76	15	415	407	376	0.13	794	775.9	0.98
72	77	18	415	407	376	0.11	875	800.2	0.91
73	78	21	421	407	382	0.09	662	647.1	0.98
74	79	14	421	407	382	0.14	591	596.9	1.01
75	80	15	415	407	382	0.13	657	775.9	1.18
76	81	18	415	407	382	0.11	713	800.2	1.12
77	82	21	421	407	381	0.09	318	331.2	1.04
78	83	18	421	407	381	0.11	304	325.6	1.07
79	Yoshizaki-165	24	433	433	333	0	102	70.7	0.69
80	Yoshizaki-166	24	433	433	343	0	147	128.1	0.87
81	Yoshizaki-167	24	433	433	343	0	135	90.0	0.67
82	Yoshizaki-168	24	433	433	345	0	159	128.1	0.81
83	Yoshizaki-169	24	433	433	345	0	175	165.9	0.95
84	Yoshizaki-170	25	433	433	333	0	160	123.7	0.77
85	Yoshizaki-171	25	433	433	343	0	235	200.3	0.85
86	Yoshizaki-172	25	433	433	343	0	220	149.2	0.68
87	Yoshizaki-173	25	433	433	345	0	269	200.3	0.74
88	Yoshizaki-174	25	433	433	345	0	275	250.0	0.91
89	Yoshizaki-176	26	433	433	343	0	322	288.1	0.89
90	Yoshizaki-177	26	433	433	345	0	279	211.1	0.76
91	Yoshizaki-178	26	433	433	345	0	382	288.1	0.75
92	Yoshizaki-179	26	433	433	351	0	422	354.2	0.84

93	WSL1	29	604	604	438	0	349	274.5	0.79
94	WSL2	29	604	604	438	0	233	274.5	1.18
95	WSL5	29	446	446	438	0	357	249.8	0.70
96	WSL7	29	604	604	438	0	324	358.5	1.11
97	WSL8	29	632	632	438	0	292	301.8	1.03
98	SW11	42	520	470	470	0	260	261.0	1.00
99	SW12	43	520	470	470	0.1	340	288.6	0.85
100	SW13	32	520	470	470	0.2	330	290.6	0.88
101	SW14	34	520	470	470	0	265	250.5	0.95
102	SW15	35	520	470	470	0.1	320	274.7	0.86
103	SW16	41	520	470	470	0.2	355	310.7	0.88
104	SW17	39	520	470	470	0	247	257.2	1.04
105	SW22	40	520	470	470	0.1	150	203.5	1.36
106	SW23	38	520	470	470	0.2	180	213.5	1.19
107	SW31	28	520	470	470	0	116	101.3	0.87
108	SW32	43	520	470	470	0	111	111.0	1.00
109	SW32R	31	520	470	470	0	83	103.3	1.24
110	SW33	39	520	470	470	0	112	108.5	0.97
111	SW33R	30	520	470	470	0	94	102.6	1.09
112	C30-N-ALR01	29	289	601	601	0.12	252	287.3	1.14
113	C30-N-ALR02	26	289	601	601	0.22	245	301.2	1.23
114	SW11	35	462	462	462	0	1850	1954.7	1.06
115	SW12	35	462	462	462	0	1737	1528.0	0.88
116	SW2	48	434	434	434	0	2342	2522.9	1.08
117	SW3	54	434	434	434	0	1888	2347.5	1.24
118	SW5	30	462	462	462	0	2831	2586.8	0.91
119	SW6	26	462	462	462	0	2184	2097.4	0.96
120	SW7	26	462	462	462	0	1323	1530.6	1.16
121	SW8	24	462	462	462	0	2600	2739.4	1.05
122	SW9	30	462	462	462	0	2791	2481.4	0.89
123	SW10	32	462	462	462	0	2275	2339.0	1.03
124	test1	26	424	424	448	0	703	509.5	0.72
125	test4	44	424	424	448	0	801	663.4	0.83
126	test2	31	424	424	448	0	467	546.5	1.17
127	test3	31	424	424	424	0	520	546.5	1.05
128	test9	30	424	424	424	0	405	455.4	1.12
129	test7	32	424	424	424	0.05	654	534.9	0.82
130	test8	32	424	424	424	0.05	707	534.9	0.76
131	test5	28	424	424	424	0.1	753	553.6	0.74
132	test6	31	424	424	424	0.1	819	587.0	0.72
133	SW4	37	550	550	500	0	105	91.6	0.87
134	SW7	32	550	550	540	0	129	90.6	0.70
135	SW8	46	400	550	540	0	95	72.2	0.76
136	SW9	39	400	550	540	0	98	95.0	0.97
137	Wall-1	25	425	435	435	0	573	573.7	1.00
138	Wall-2	22	425	435	435	0	680	759.7	1.12
139	Wall-7	45	450	450	450	0	380	499.3	1.31
140	Wall-8	45	450	450	450	0	225	336.3	1.49
141	WR-20	28	342	342	449	0.1	442	539.9	1.22
142	WR-10	28	342	342	449	0.1	425	539.9	1.27
143	WR-0	28	342	342	449	0.1	424	539.9	1.27
144	W4	33	480	480	480	0	400	557.6	1.39
145	W5	27	480	480	480	0	600	669.4	1.12
146	B14CD8U	40	450	450	450	0	480	616.3	1.28
147	SW2	48	414	414	414	0	2504	2849.9	1.14
148	SW3	54	414	414	414	0	2082	2487.8	1.19

149	T01	24	420	420	420	0	107	145.0	1.35
150	T04	29	0	420	420	0	90	84.2	0.94
151	T05	24	420	420	420	0	127	145.0	1.14
152	T11	27	500	500	500	0.07	129	180.3	1.40
153	MSW5	22	610	610	585	0	187	219.4	1.17
154	LSW1	22	598	598	585	0	262	337.8	1.29
155	LSW2	22	610	610	585	0	191	225.1	1.18
156	LSW3	24	610	610	585	0.07	268	260.4	0.97
157	LSW4	23	610	610	585	0	232	228.6	0.99
158	LSW5	25	610	610	585	0	247	235.6	0.95
159	W9	31	588	604	604	0	177	205.0	1.16
160	W11	31	588	604	604	0	173	172.3	1.00
161	W13	25	588	604	604	0	158	162.6	1.03
162	T2-S2-3	26	481	481	440	0	666	568.3	0.85
163	T2-S3-4	29	584	584	473	0	813	656.5	0.81
164	T4-S1-6	35	584	584	519	0	874	771.3	0.88
165	T5-S1-7	35	584	584	528	0	710	559.4	0.79
166	T6-S1-8	23	584	584	528	0	735	568.6	0.77
167	T1-S2-9	24	584	584	473	0	563	429.3	0.76
168	SW23C2	33	478	478	538	0.14	83	104.8	1.26
169	SW60N1	33	469	469	465	0.07	105	112.5	1.07
170	SW60N2	33	469	469	465	0.14	110	122.8	1.12
171	SW60C1	33	469	469	465	0.07	110	112.5	1.02
172	SW60C2	33	469	469	465	0.14	117	122.8	1.05
173	RW-A20-P10-S38	47	516	450	472	0.07	405	422.0	1.04
174	RW-A20-P10-S63	49	443	443	477	0.07	742	624.3	0.84
175	RW-A15-P10-S51	49	516	450	472	0.08	603	500.2	0.83
176	RW-A15-P10-S78	56	443	443	476	0.06	859	703.6	0.82
177	RW-A15-P2.5-S64	58	443	443	476	0.02	670	612.1	0.91
178	Wall 1	36	464	464	464	0	1618	2296.6	1.42
179	Wall 2	37	464	464	464	0	1705	2318.6	1.36
180	SH–CFP–M	43	563	600	600	0	548	654.6	1.19
181	SH–DCM–M	43	563	600	600	0	624	654.6	1.05
182	SH–CFP–C	43	563	600	600	0	537	654.6	1.22
183	SH–DCM–C	43	563	600	600	0	555	654.6	1.18
184	H0.1S	41	642	641	617	0.08	394	276.8	0.70
185	U1.0-BC	31	520	520	520	0.07	415	422.6	1.02
186	U1.0-BC2	34	520	520	520	0.07	368	434.1	1.18
187	Ohono_1-2	29	224	224	224	0	204	162.4	0.80
188	M4	24	745	504	504	0.05	135	182.3	1.35
189	C1.0	35	520	520	520	0.07	455	419.1	0.92
								AVG	1.02
								COV	0.20